Influence of SO_2 on CO_2 transport by pipeline for carbon capture and storage (CCS) technology: Evaluation of CO_2/SO_2 co-capture

Beatriz Gimeno, Manuela Artal, Inmaculada Velasco, Javier Fernández and Sofía T. Blanco*

Departamento de Química Física, Facultad de Ciencias, Universidad de Zaragoza, 50009 Zaragoza, Spain

ABSTRACT: CO_2 capture and storage (CCS) is an important technology for avoiding atmospheric CO_2 emissions, which are principally originated from fossil fuels combustion. Anthropogenic CO_2 contains impurities that can strongly modify the properties of the stream. Several authors have showed that some of these impurities, such as SO_2 present in emissions from sulfur containing fuels, could be favorable for some steps of the process, and the possibility of co-capture has been proposed. To assess this possibility with regard to the transport stage of CCS, we determined the influence of SO_2 on selected parameters of transport by pipeline (minimal operational pressure, pressure and density drops, distance between boosters, booster power, and inner diameter of the pipeline and the Joule-Thomson coefficient). For this purpose, we obtained new and accurate experimental data for the density and vapor-liquid equilibrium of five CO_2+SO_2 mixtures under conditions of interest for CCS and speed of sound data for four of them. We compared our results with those found in the literature and with the values calculated

using two equations of state for their validation: PC-SAFT and an extended version of EOS-CG that includes a binary model for the CO_2+SO_2 mixture. Allowing for the fact that chemical effects due to the presence of SO_2, such as pipeline corrosion, have not been considered, we conclude that CO_2/SO_2 co-capture might favor and decrease the costs of the transport step of this technology, helping to avoid emissions of a highly toxic gas to the atmosphere without high desulfuration expenses.

1. INTRODUCTION

The globally averaged monthly mean concentration of CO_2 in the atmosphere overtook the symbolic barrier of 400 ppm in March 2015.[1] This value is 15% higher than the recommended upper limit of 350 ppm to avoid dangerous climate change.[2,3] Nonetheless, the annual mean global CO_2 growth rates in 2015 and 2016 were the highest ever measured (3.01 and 2.98 ppm/year), and, after an increment of 1.95 ppm in 2017, the average CO_2 concentration was 407.5 ppm in April 2018.[1] The central aim of the Paris Agreement[4] is to mitigate climate change by keeping the global temperature rise this century less than 2°C above pre-industrial levels (2 degrees scenario, 2DS). Moreover, this agreement pursues efforts to limit the temperature increase even further to 1.5°C. At minimum, this scenario requires maintaining the global CO_2 concentration below 450 ppm throughout the century,[5] but at the current rate of growth, this level will be reached before 2040.

Emissions of CO_2 from stationary sources arise mainly from fossil fuel combustion in the power generation sector, and significant amounts of CO_2 are produced as well in the oil and gas processing industrial sectors.[6] Given that the use of fossil fuels is not expected to decrease in the next few decades and that the production of anthropogenic CO_2 is expected to grow, CCS (carbon capture and storage) appears to be one of the most important technologies for avoiding

CO_2 emissions to the atmosphere and thus mitigating climate change. In the case of the power generation sector, many sources have large emission volumes that make them amenable to the addition of CO_2 capture technology. CCS consists of the capture of anthropogenic CO_2 at the emitting power plants or industrial sites, its conditioning, its transport, and finally its injection and storage underground. CO_2 capture can be achieved using different techniques, such as postcombustion, precombustion, and oxy-fuel combustion. Conditioning is carried out by dehydration, non-condensable gas separation and/or liquefaction, and compression-pumping.[6-9] For transport, the use of high-pressure pipelines is accepted as the most practical method to move large amounts of CO_2 over long distances.[10-13] The fluid is transported in the dense or supercritical phase, thereby avoiding phase changes and two-phase flow, which produces cavitation and turbulence and reduces the quantity of fluid transported.[14] Although transporting CO_2 in the gaseous phase may be useful for low mass flow rates and short distances,[15] this case was not considered in this work. The storage occurs in geological reservoirs, such as depleted oil and gas fields, deep saline aquifers or deep unmineable coal seams.[16]

It is impossible to implement least-cost emissions reduction scenarios, consistent with the Paris Agreement, that do not include wide deployment of CCS.[5] International Energy Agency (IEA) and Global CCS Institute projections indicate that 2DS would require the capture and storage of approximately 4 Gt per year of CO_2 in 2040, which is about 100 times the annual CO_2 capture capacity expected to be in operation by 2018; in 2050, the amount required to be stored will be of 5 Gt per year.[17,18] To reach these targets, a rapid acceleration of current CCS deployment will be essential. First estimations indicate that between 200,000 and 360,000 km of high-pressure CO_2 pipelines will be required worldwide in 2050.[19] Comparatively, the currently existing

network comprises approximately 6,500 km of pipelines, most of which are dedicated to enhanced oil recovery and located in the USA.[20]

It is well known that the fluid transported in these pipelines, anthropogenic CO_2, contains impurities such as N_2, H_2, O_2, Ar, SO_2, NO_x, CO, CH_4 and H_2O that are derived from the emission sources and the capture and conditioning processes.[21,22] The presence of these impurities, even at low concentrations, can strongly affect the properties of the fluid (density, ρ; vapor-liquid equilibrium, VLE; speed of sound, c; viscosity, η; etc.) and therefore the pipeline hydraulics and the design and operation of the pipeline network. Thus, knowledge of the properties of the impure stream is essential to determine the required purification level and to study the possibility of co-capturing impurities with CO_2. Increasing the purity of CO_2 could prevent potential risks such as pipeline corrosion and could provide streams with properties more similar to those of pure CO_2; however, purification greatly increases the costs of the process. High-level purification is technically available but economically infeasible.[8] Moreover, purification may not always be desirable. Several authors [23-32] have suggested that the presence of certain impurities, such as SO_2 generated in case of sulfur containing fuels, may favor some steps of the CCS process, mainly due to the effect of SO_2 on the density and the Joule-Thomson coefficient of the fluid. Additionally, CO_2/SO_2 co-capture helps avoid the emission of SO_2 into the atmosphere. Thus, the viability of the CO_2/SO_2 co-capture is an interesting issue worthy of being studied. However, we have not found literature reports on the effect of SO_2 on the hydraulic and thermodynamic aspects of transport for CCS, and experimental data on the CO_2+SO_2 system are very limited. This could be due to the risks to researchers and facilities arising from the toxicity of SO_2.

This work is a part of a wider project that studies the feasibility of CO_2/SO_2 co-capture, focusing on the transport, injection and storage steps and on the simultaneous presence of other impurities, such as CO and CH_4. Its first aim was to study those CO_2+SO_2 mixtures with compositions, temperatures and pressures of interest for CCS technology. We previously published two papers[33,34] on experimentally determining the thermodynamic properties of these mixtures at temperatures and pressures relevant to injection and storage. We found that the presence of SO_2 is profitable in most of the considered aspects (permeation flux, reservoir capacity, rising velocity of the plume inside deep saline aquifers and cooling during fluid expansion) especially in the case of shallow reservoirs. Now, in this work, the temperatures and pressures studied are relevant to the transport step. In this regard, we experimentally determined new and accurate pressure-density temperature, $p\rho T$, and VLE data for five CO_2+SO_2 mixtures, as well as pcT for four of them (given that the speed of sound of the remaining mixture was previously published,[33] although it is included in the discussion of this work). The studied compositions (mole fraction of CO_2, x_{CO_2}) range from 0.80 to 0.99, including a proposed co-capture mixture of 0.95 that is particularly considered throughout this work.[25] The working temperatures vary from 263 to 304 K. Pressures reach up to 20 MPa for densities and up to 190 MPa for speeds of sound. These ranges include the conditions of interest for the pipeline transport step of CCS and extend them to improve the knowledge of the behavior of the system and to reach the second aim of the work: equation of state (EoS) validation over broader ranges than those found in CCS. Given the wide ranges of compositions, pressures and temperatures involved in CCS processes, an accurate predictive tool such as an EoS will be extraordinarily useful. In this paper, we contribute to finding such a predictive tool by comparing our experimental data with those provided by two EoS of different formulations: an extended EOS-

CG, and PC-SAFT.[35] The extended EOS-CG is a recent and unpublished version of the original EOS-CG[36] that covers the CO_2+SO_2 mixture (absent in the original model) which is used as implemented in the TREND 2.0.1 software.[37]

The speed of sound of the CO_2+SO_2 mixtures with $x_{CO_2} \geq 0.9$ can not be determined in our device, due to the acoustical opacity of CO_2 at 5 MHz.[33] To obtain proper signals, we doped the mixtures with small amounts of methanol, following a previously tested method.[33] In the low-pressure range, where signals were not obtained despite the doping, we used our experimental data to obtain extrapolated speed of sound values, which were validated by comparisons with the values obtained from the EoS.

Finally, as the third aim of the work, we determined several parameters related to the transport step of CCS technology, and we demonstrated the effect of the presence of SO_2 on them to evaluate the possibility of co-capture: minimum operational pressure; pressure and density drops along the pipeline, $p(d)$ and $\rho(d)$, respectively; maximum repressurization distance, L; power of the booster stations, W; and inner diameter of the pipeline, D. In addition, we calculated the Joule-Thomson coefficient, μ_{JT}, of the mixtures, which determines the thermal behavior of the fluid during depressurization, either operational or accidental, and is therefore important in both operations and hazard and risk studies.

Only the thermodynamic and hydraulic aspects were taken into account in this work; the chemical effects due to the presence of SO_2, such as the possibility of pipeline corrosion, primarily in the presence of water,[29,38-46] were not considered. It is well known that, while dry CO_2 does not react with steel, the presence of water, even in small amounts, highly increases corrosion. Moreover, if the stream contains other impurities, they will contribute according to their nature and concentration. SO_2, in presence of water, leads to sulfurous acid, and, in

presence of oxygen, SO_2 can be oxidized to sulfur trioxide and sulfuric acid can be formed. Even if it is clear that the presence of SO_2 intensifies the corrosiveness of wet CO_2, some authors have shown that corrosion is lower than expected, adducing principally the formation of protective layers of iron sulfate/sulfite hydrates[40] and the low mobility of sulfuric acid in supercritical CO_2.[42] In which authors agree is that the determining factor for corrosion is the amount of water, and some of them claim that reducing water content is a more favorable option compared to reducing SO_2 content to minimize corrosion.[46] Corrosion is important, but also other effects have to be considered. The assessment of the viability of CO_2/SO_2 co-capture must be carried out taking into account thermodynamic, hydraulic, and chemical effects. Conclusions must be derived from the balance of all of them, including technical, economic, and safety factors, as well as environmental considerations.

All the evaluations were performed in this work using new and accurate experimental values for the pressure−density−temperature composition, $p\rho Tx_{\mathrm{CO_2}}$, and VLE and experimental and extrapolated values for the pressure−speed of sound−temperature−composition, $pcTx_{\mathrm{CO_2}}$, of CO_2-rich mixtures containing SO_2. Thus, to the best of our knowledge, this work constitutes so-far the most comprehensive study on the impact of SO_2 on thermodynamic and hydraulic aspects of CCS transport based on experimental data. The results reported are necessary to establish the quality requirements/specifications of anthropogenic CO_2 and to provide realistic values of the parameters needed for the safe and efficient design and operation of the pipeline network. All this information is essential to reach the needed deployment of CCS to accomplish the 2DS in the medium term.

2. EXPERIMENTAL SECTION

2.1. Materials. Carbon dioxide and sulfur dioxide (mole fraction > 0.99998 and 0.9990, respectively) were purchased from Air Liquide and used as received. Methanol (biotech grade, mole fraction 0.9993) from Sigma Aldrich was degassed immediately before use.

2.2. Apparatus and methods. Given the toxicity of SO_2, even in small amounts, and the inherent risk of working under high-pressure conditions, the laboratory was equipped with the necessary safety measures: all apparatuses were enclosed by safety polycarbonate panels, and fume hoods, gas masks, supplied-air hoods and gas detectors were used.

The mixtures were prepared in a variable volume cell manufactured by Top Industrie S.A.S. with a maximum volume of 0.51 L and a maximum working pressure of 30 MPa, as described previously.[34] The components of the mixture were introduced into the cell in the order of increasing volatility. For mixtures with methanol (a dopant used, when necessary, for speed of sound determination), this component was added into the evacuated cell first and then degassed via intermittent vacuum with agitation for three hours. The masses of the different components were determined by successive weighing of the cell in a mass comparator Sartorius CCE 2004, with repeatability better than 0.0002 g. The standard uncertainty in the mole fraction, u_x, was determined to be 2×10^{-4}.[34]

To obtain the $p\rho T$ experimental data, we used an installation with an Anton Paar DMA HPM vibrating-tube densimeter connected to an MPDS V3 evaluation unit as the main component.[47,48] It operates at temperatures T from 263 to 423 K and at pressures p from atmospheric pressure to 70 MPa. The temperature uncertainty, u_T, is of 0.006 K and the pressure uncertainty, u_p, is 0.0015 MPa for $p < 6$ MPa and 0.018 MPa for 6 MPa $\leq p \leq$ 70 MPa. The probes used to measure

the temperature were calibrated by the Centro Español de Metrología, CEM,[49] and the pressure transducers were calibrated in our laboratories via a WIKA CPH 6000 calibrator.[34]

The quasi-continuous acquisition of the data (approximately 6000 $p\rho T$ points per isotherm, evenly reduced to approximately 1000 for easier handling) is achieved using a fluid flow of 0.005 MPa·s^{-1}, which allows measurements at thermodynamic quasi-equilibrium, as the designers of the apparatus indicate.[50] A detailed explanation of apparatus and procedures can be found in previous publications.[34,47,48] The high number of points with small separations allows the determination of the limits of the vapor-liquid equilibrium and the derivative properties from the experimental data.

The stability of the temperature during the measurement of each $p\rho T x_{\mathrm{CO_2}}$ isotherm was better than ± 0.05 K. The experimental combined uncertainties in ρ, u_ρ, were calculated using the propagation uncertainty law according to the procedure detailed in a previous publication.[34] These values are included in the tables of results, and their global average value was 0.49 kg·m^{-3}. The procedure to determine the VLE limits, p_{dew} and p_{bubble}, and the densities of the vapor, ρ_{V}, and liquid, ρ_{L}, phases in the VLE and the calculation of their uncertainties were based on the methods proposed by the designers of the experimental setup[50] and are explained elsewhewe.[34] The combined uncertainties in the VLE data, which are reported in the tables of results, exhibit global average values of 0.017 MPa for pressure and 1.1 kg·m^{-3} for density.

The speed of sound measurements were performed with an installation that employs a 5 MHz pulsed ultrasonic system.[33] It allows measurements in liquids and in compressed gases in the dense or supercritical phase. The main component is a dual-path ultrasonic cell located within a pressure vessel inside a thermostatic bath. The apparatus works from 253 K to 473 K with a

temperature uncertainty, u_T, of 0.015 K. The maximum achievable pressure is 200 MPa, and the u_p is 0.02 MPa.

The mixtures with greater than 90 mole % of CO_2 were found to be opaque to sound at 5 MHz. Consequently, we doped them with ≅ 0.8 mole % methanol in order to obtain proper signals. This method was tested in a previous work.[33] In that study, which was conducted on the CO_2+SO_2 mixture with x_{SO_2} = 0.1032 in the same *T* and *p* ranges as in this work, we showed that the difference in *c* between the doped and the undoped mixtures is small in terms of experimental results (0.17% on average) and is negligible for modeling

The combined uncertainties in *c*, u_c, calculated using the propagation uncertainty law according to the procedure described in a previous paper,[34] were $u_c = 6.2 \times 10^{-4} c$ for CO_2+SO_2 and $u_c = 8.1 \times 10^{-4} c$ for CO_2+CH_3OH+SO_2.

3. RESULTS AND DISCUSSION

The experimental and extrapolated thermodynamic results obtained in this work are shown in this section (subsection 3.1); they are subsequently compared to those calculated with the extended EOS-CG and PC-SAFT EoS in order to evaluate their predictive capability (3.2) and used to determine the influence of SO_2 on several transport parameters (3.3) and on the Joule-Thomson coefficient of the fluid (3.4).

3.1. Results. We measured 20 $p\rho T x_{CO_2}$ isotherms (4 isotherms per mixture) for five CO_2+SO_2 mixtures (CO_2 mole fraction x_{CO_2} = 0.8029, 0.8969, 0.9532, 0.9698, and 0.9931) at temperatures *T* = 263.15, 273.15, 293.15, and 304.21 K and pressures up to 20 MPa. This provides a total of ≅ 20,000 points, which are available in the Supporting Information, SI, Table S1. A reduced number of points is presented in Table 1. The corresponding graphics are shown in Figures 1 and S1 (SI). The *T* and *p* ranges were chosen considering the operating conditions

during transport by pipeline.[20,51,52] The range of compositions encompasses a possible co-capture mixture[25] ($x_{CO_2} = 0.9532$) and spans from a mixture with $x_{CO_2} = 0.8029$ to CO_2-rich mixtures more similar to industrial emissions[53,54] to extend the validation range for the EoS and enhance the general understanding of the impact of SO_2.

The presence of SO_2 increases the density of the mixture relative to that of pure CO_2[55] under all the studied conditions, and the ρ values of the mixtures increase with increasing x_{SO_2} and pressure and with decreasing temperature. All the studied isotherms were subcritical, and we used the experimental data to obtain the dew and bubble pressures, p_{dew} and p_{bubble}, and the densities of the phases in equilibrium for vapor, ρ_V, and liquid, ρ_L. The results are collected in Table S2 and presented in Figures 2, S2 and S3. For comparison, Table S2 and Figure 2 also include the saturation pressures, phase densities, or critical data of pure CO_2.[55,56]

In the literature, we found only one reference on experimental volumetric data for CO_2+SO_2 under the studied conditions. Nazeri et al. (2017)[32] presents pressure-temperature-density data for a mixture with $x_{CO_2} = 0.9503$ at 273 and 283 K, and for a mixture with $x_{CO_2} = 0.9478$ at 298 K, at pressures up to approximately 42 MPa. The first composition is very close to our mixture with $x_{CO_2} = 0.9532$, even though the difference is higher than the experimental composition uncertainties reported in both works. The 273 K temperature is also very similar to one of this work (273.15 K), but again the difference is higher than the temperature uncertainties: Nazeri et al. measured nine experimental points in the vapor phase at 272.65 K and 77 points in the liquid phase between 273.54 and 273.60 K. Our experimental density data (about 1000 experimental points, including both phases) were measured at 273.15±0.05 K. The deviations, expressed as *MRD*, are very small along the coincident range of pressure: 0.85% for the vapor phase and

0.46% for the liquid phase, with an average value of 0.54%. The rest of the data presented by Nazeri et al., even if not directly comparable, are in good agreement with ours.

About VLE experimental data, several references were found.[32,34,57-62] The data from Coquelet et al. at 263.15 and 333.15 K[62] are the only values reported by the NIST Standard Reference.[63] Data at 263.15 K, which are represented in Figures 2 and S2, include a bubble point and a dew point which can be compared exactly with our results since the temperatures and compositions match. The average difference in pressure is 1.3%. The rest of the points from Coquelet et al. obtained at 263.15 K show good agreement with our data (Figures 2 and S2). Nazeri et al.[32] give two bubble points for their mixture with $x_{CO_2} = 0.9503$, at 273.56 and 283.33 K. At 273.56 K, the reported bubble pressure is about 7% higher than our bubble pressure for x_{CO_2}=0.9532 at 273.15 K (Figure 2). However, liquid phase densities at equilibrium are very similar, with a difference of 0.16%. The values for both properties at 283.33 K are not directly comparable with ours, but they are in good agreement. The data from Gimeno et al.[34] were measured at the same compositions and higher temperatures than ours and are in good agreement with our results (Figures S2, S3). Caubet[58] determined several bubble points for a mixture with x_{CO_2} = 0.8866 at temperatures ranging from 295.15 K to 313.95 K, as well as some dew points from 300.15 K to 322.95 K for the aforementioned mixture and from 299.15 K to 310.15 K for a mixture with x_{CO_2} = 0.9265. None of these points are directly comparable to those in this work because of the different composition and/or temperature, but they are consistent with our data. The VLE data from Bluemcke[57] and Thiel et al.[59] correspond to mixtures with more dilute CO_2 than ours. The experimental data in Cummings[60] and Lachet et al.[61] are the same as those from Caubet[58] and Coquelet et al.,[62] respectively.

We determined 16 $pcTx_{CO_2}$ isotherms (four isotherms per mixture) for one CO_2+SO_2 and three CO_2+CH_3OH+SO_2 mixtures, all of which had the same SO_2 mole fractions, x_{SO_2}, as four of the five mixtures for which the density was determined (x_{SO_2} = 0.1971, 0.0468, 0.0302, and 0.0069) at the same temperatures T = 263.15, 273.15, 293.15, and 304.21 K and at pressures up to 190 MPa (Table S3, Figure 3, Figure S4). The data for the mixture with x_{SO_2} = 0.1031 were previously published,[33] and they are discussed below. Given that the three mixtures with $x_{SO_2} <$ 0.1 were essentially opaque to sound in most of the studied range of pressures, we doped them with ≅ 0.8 mole % of methanol to obtain proper signals according to the method described in Rivas et al. (2016).[33] The lower pressure limit of each isotherm was determined based on the point at which sound absorption became too large to receive the signal.

For each composition and temperature, a polynomial model was fitted to the experimental speed of sound measurements:[33]

$$(p - p^{\#}) = \sum_{i=1}^{3} a_i (c - c^{\#})^i \qquad (1)$$

where $p^{\#}$ is a reference pressure appropriate for each isotherm and $c^{\#}$ is the speed of sound at p = $p^{\#}$. Table S4 shows the coefficients for eq. (1), the values of $p^{\#}$, and the mean relative deviations, MRD_c (%), between the experimental and fitted values. The overall mean relative deviation was $\overline{\overline{MRD_c}}$ = 0.010%, which is lower than the relative combined uncertainty of the experimental data.

Most of the lowest values of pressure of the $pcTx_{CO_2}$ isotherms are higher than the usual pressure range during transport by pipeline. For this reason, polynomials (1) with coefficients from Table S4 were used to extrapolate the c values to the low-pressure region where no signal was obtained. The extrapolated values are reported in Table S5 and Figure 3 and were validated with the two studied EoS, as explained in the next section.

The c values in the mixtures vary with T, p and x_{SO_2} in a similar way to the density, increasing with increasing x_{SO_2} and pressure and with decreasing temperature. We found no literature data for the speed of sound in the CO_2+SO_2 and CO_2+CH_3OH+SO_2 systems.

3.2. Comparison of the data with models. The fluids handled in CCS technology are CO_2-rich mixtures with different impurities at variable concentrations and are used in wide ranges of pressure and temperature. Predictive tools such as EoS are required to obtain adequate knowledge of their properties.[51,64-66] Recently, a new EoS based on the basic mathematical approach of the GERG EoS[67] was developed principally for application to humid gases, combustion gases and CO_2-rich mixtures of interest for CCS: the original EOS-CG mixture model.[36] This original model does not include SO_2. In this work, we evaluate both an unpublished extended EOS-CG that includes a binary model for the CO_2+SO_2 mixture and the PC-SAFT EoS,[35] which is widely used for calculations of thermodynamic properties, by comparing the values obtained from them with our experimental data. The differences are presented as the mean relative deviations, MRD_X. The methanol-doped mixtures used for c measurements were modeled as pseudo-binary CO_2+SO_2 mixtures with the same SO_2 concentrations: the mole fractions of SO_2 used were those existing in the ternary mixtures, x_{SO_2}, and the mole fractions of CO_2 were considered to be $x_{CO_2} = 1\text{-}x_{SO_2}$.

The EOS-CG was applied as implemented in TREND 2.0.1 software (Thermodynamic Reference & Engineering Data).[37] In TREND the original EOS-CG model of Gernert and Span[36] is extended to additional minor components of typical CCS-mixtures. The implemented binary model for CO_2+SO_2 was developed at Ruhr University Bochum and is so-far unpublished. Due to the limited amount of experimental data that was available prior to our publication, the binary model contains only two adjusted parameters (of the temperature reducing function). For the CO_2

and SO_2 pure fluids, the model uses the Span and Wagner[55] and the Gao et al.[68] EoS respectively. The MRD_X values are shown in Tables S6 and S7 and in Figures S5 and S6. The MRD_ρ values decreased upon increasing the mole fraction of CO_2 and did not show a clear trend with the temperature; the global average value was $\overline{\overline{MRD_\rho}} = 0.54\%$. Regarding the VLE, $\overline{\overline{MRD}}_{p_{dew}}$ = 2.07%, $\overline{\overline{MRD}}_{p_{bubble}}$ = 0.88%, $\overline{\overline{MRD}}_{\rho_V}$ = 2.91%, and $\overline{\overline{MRD}}_{\rho_L}$ = 0.73%. The mean relative deviations on densities of the phases at equilibrium do not include the mixture with x_{CO_2}= 0.9931 at 304.21 K. Although the dew and bubble pressures of this mixture are well reproduced (deviations of 0.87% and 0.61%, respectively), the EoS shows anomalous behavior in the prediction of the phase densities with very high deviations from our experimental data (25.6% for vapor and 9.46% for liquid), which is probably due to the close proximity to the critical point of the mixture. Figures 2, S2 and S3 include the experimental VLE data from this work and Coquelet et al.[62] and those calculated from the extended EOS-CG at the studied temperatures. When we compared the deviations between our experimental *c* data and those calculated by the EoS, we did not find remarkable trends with the temperature or composition, and the global average value was $\overline{\overline{MRD_c}} =$ 0.40%. For the extrapolated values, $\overline{\overline{MRD_c}} = 0.39\%$.

The calculations with the PC-SAFT EoS were performed using VLXE software.[69] The methodology employed was previously described,[33] and a volume translation parameter, Δv_c, was added to better reproduce the density values.[34,70] We took a binary interaction parameter from the literature[71] since using a binary interaction parameter obtained from fitting our experimental data did not significantly modify the results. The pure compound parameters, the binary interaction parameters and the Δv_c values are listed in Table S8, and the MRD_X values are shown in Tables S6 and S7 and Figures S5 and S6. The MRD_ρ increased with the increasing temperature, and there was no clear trend with the composition. The global average value was

$\overline{\overline{MRD_\rho}} = 0.56\%$. Regarding the VLE, $\overline{\overline{MRD}}_{p_{dew}}$ = 2.44%, $\overline{\overline{MRD}}_{p_{bubble}}$ = 1.07%, $\overline{\overline{MRD}}_{\rho_V}$ = 2.77%, and $\overline{\overline{MRD}}_{\rho_L}$ = 0.64%. Comparison of the experimental VLE results with these EoS predictions is shown in Figures 2, S2 and S3. MRD_c relative to the experimental results decreased with increasing T and increased with increasing x_{CO_2} with a global average value of $\overline{\overline{MRD_c}} = 3.71\%$. In the extrapolated results, MRD_c increased with increasing T and with decreasing x_{CO_2}, and $\overline{\overline{MRD_c}} = 3.70\%$.

In a recent publication, Xu et al.[72] presented thermodynamic calculations for the CO_2+SO_2 system using the PC-SAFT EoS but with different parameters from those utilized in this study. Comparing our experimental data with those calculated using the PC-SAFT EoS and the parameters from Xu et al., we found the following deviations: $\overline{\overline{MRD_\rho}} = 0.93\%$, $\overline{\overline{MRD}}_{p_{dew}}$ =4.10%, $\overline{\overline{MRD}}_{p_{bubble}}$ = 1.82%, $\overline{\overline{MRD}}_{\rho_V}$ = 6.26%, $\overline{\overline{MRD}}_{\rho_L}$ = 0.71%, and $\overline{\overline{MRD_c}} = 2.46\%$. These deviations were higher than those obtained using the parameters from Table S8, except for the deviation in speed of sound.

3.3. Influence of SO_2 on transport. Studies about the chemical effect of SO_2 on the transport of the CCS stream, especially in the presence of water, can be found in the literature.[38-46] However, we were unable to find studies about how SO_2 influences pipeline design and operating parameters. In this work, we paid attention to the influence of the presence of SO_2 on the transport of anthropogenic CO_2 by pipeline. This was achieved by calculating the minimum operational pressure and several selected transport parameters related to this step of the CCS technology: pressure and density drops along the pipeline, $p(d)$ and $\rho(d)$; maximum repressurization distance (maximum separation distance between boosters), L; power of the booster stations, W; and inner diameter of the pipeline, D. These parameters, as well as other

required ones (Reynolds number, *Re*; friction factor, *f*; and pressure drop per meter, $\Delta p/d$), were calculated using the equations presented in Table S9, which have been reviewed and accepted by the industrial and engineering community.[73,74] For these calculations, we used our experimental ρ values, whereas the needed viscosity values of the mixtures were calculated using an improved extended corresponding states method for estimation of viscosity[75] as implemented in the REFPROP 9.1 software,[76] due to the lack of experimental data. In addition, we calculated the Joule-Thomson coefficient, μ_{JT}, via the equations:

$$\mu_{\mathrm{JT}} = \left(\frac{\partial T}{\partial p}\right)_H = \frac{V}{C_p}\left(\alpha_p T - 1\right) \tag{2}$$

$$C_p = \frac{\alpha_p^2 T}{\rho(\kappa_T - \kappa_S)} \tag{3}$$

where V is the molar volume, C_p is the heat capacity at constant pressure, and α_p, κ_T, and κ_S are the isobaric thermal expansivity and isothermal and isentropic compressibility, respectively. α_p was calculated from our experimental density data (263.15 K – 304.21 K); to improve the calculations at the temperatures of the extremes of the interval, experimental values from Gimeno et al.[34] at 313.15 K and values calculated using the extended EOS-CG at 253.15 K were also used. κ_T was obtained from the experimental ρ values, and κ_S was determined from the experimental ρ data and experimental and extrapolated c data. For pure CO_2, these properties were obtained using the reference EoS of Span and Wagner[55] as implemented in REFPROP 9.1.[76] The Joule-Thompson coefficient is necessary for understanding the thermal behavior of the fluid in pipeline depressurization or release (operational or accidental) because its value determines whether the stream cools or warms up upon pressure drop.

All the aforementioned factors must be considered in the design and operation of the pipeline network and balanced to obtain the most practical, safe, and cost-effective conditions.

3.3.1. Minimum operational pressure. The estimated operating conditions of anthropogenic CO_2 transport by pipeline range from 7.5 to 20 MPa and from 273.15 to 303.15 K.[51] Some authors[65,77] proposed an operating pressure above 8.6 MPa to ensure that the fluid will always be in a single phase, dense or supercritical, over the whole range of temperatures that the anthropogenic CO_2 in the pipeline may experience. Nevertheless, the lower limit for the operating pressure to avoid the undesired formation of a vapor phase is given by the bubble pressure of the fluid at the transport temperature (plus a margin for safety). Table S10 shows the p_{bubble} and ρ_{L} of the studied mixtures, as well as the saturation pressures of pure CO_2 at the same temperatures[55] and the critical point of pure CO_2.[56] Clearly, the presence of SO_2 causes the bubble pressure of the fluid to diminish at a given temperature, allowing transport at lower pressures. The effect increases with increasing temperature. For the proposed co-capture mixture ($x_{\text{CO}_2} = 0.9532$), the differences in pressure with respect to pure CO_2 were 4.5% at 263.15 K and 7.2% at 293.15 K.

Instead of a minimum pressure, other studies propose a minimum reference value for the density of the transported fluid, suggested to be 800 kg·m^{-3}.[73,74] Fifteen of the twenty studied isotherms-isopleths present ρ_{L} values above 800 kg·m^{-3} (Tables S2 and S10). Because vapor phase formation must be avoided, recompression must be carried out before reaching the bubble pressure, even if the density of the fluid is higher than the reference value of 800 kg·m^{-3}. Table S10 also includes the minimum experimental pressures to obtain densities ≥ 800 kg·m^{-3} avoiding vapor phase formation, p_{800}, and the densities at these pressures, ρ_{800}. We define p_{saf} as the minimum safe operating pressure considered in this work, and ρ_{saf} as the density at p_{saf} (Table S10). If $\rho_{\text{saf}} \geq 800$ kg·m^{-3}, then $p_{\text{saf}} = p_{800}$. If $\rho_{\text{saf}} < 800$ kg·m^{-3}, then p_{saf} will be equal to p_{bubble} plus a safety margin of 1 MPa ($p_{\text{saf}} = p_{\text{bubble}} + 1$ MPa). For comparison, the same

parameters determined for pure CO_2 are also included.[55,56] We found that all the different pressure values shown in Table S10 for the mixtures are lower than those for pure CO_2 at each temperature, thereby allowing transport at lower pressures, which is favorable for pipeline operation. The differences in p_{saf} increase as the amount of SO_2 and the temperature increase. For the co-capture mixture $x_{\mathrm{CO_2}} = 0.9532$, we observed decreases in p_{saf} compared to pure CO_2 of 3.3% at 263.15 K and 6.1% at 293.15 K.

3.3.2. Pressure, $p(d)$, and density, $\rho(d)$, profiles along the pipeline. The presence of impurities also affects the pressure drop—and therefore the density drop—along the pipeline. When the pressure or density reaches the minimum established values, repressurization is mandatory. In this paper, we work with two repressurization scenarios: when the pressure reaches a minimum value of p_{saf} at each temperature (scenario A, Table S10) and 8.50 MPa (scenario B). Figures 4 and S7 show the pressure profiles, and Figures 5 and S7 show the density profiles as a function of the distance traveled by the stream.

We considered a pipeline with intermediate characteristics among those found in the literature,[20] namely, with an inner diameter D = 0.508 m (20 inches) and a capacity (mass flow) m = 317.1 kg·s^{-1} (10 Mt/year). The inlet pressure, p_{in}, was taken as 20.00 MPa, and the roughness height used was 4.6×10^{-5} m (0.00015 ft).[52,73] No differences in altitude were taken into account in the route of the pipeline.

As seen in Figures 4, 5 and S7, both the pressure and density drop more slowly for the mixtures than for pure CO_2, which is due to their density and viscosity values. The differences are higher at higher concentrations of SO_2 and higher temperatures. For the co-capture mixture ($x_{\mathrm{CO_2}} = 0.9532$) at 293.15 K and a distance, d, of 300 km, the pressure drops from 20.00 to 10.71 MPa (46%); the density, from 964.7 to 900.9 kg·m^{-3} (6.6%). When the fluid is pure CO_2,

the pressure drops from 20 to 10.37 MPa (48%); the density, from 937.1 to 860.7 kg·m^{-3} (8.2%). The slower decreases in the fluid pressure and density favor the transport operations because they allow the stream to travel a longer distance without repressurization.

3.3.3. Maximum repressurization distance, *L*, and booster station power, *W*. The pressure drop, itself a function of the inlet pressure, the diameter of the pipeline, the mass flow, and the properties of the transported fluid, determines the placement and number of pumping (booster) stations if necessary.

Figure 6 shows the maximum repressurization distance (maximum distance between boosters), *L*, versus the transport temperature, T_{tr}, in scenarios A and B. In both scenarios, the distance before repressurization is longer for the mixtures than for pure CO_2, indicating that the transport of the mixtures is favored over that of pure CO_2. The higher the mole fraction of SO_2 and the temperature, the higher the difference in *L* between the mixtures and pure CO_2.

Comparing the two scenarios with each other shows that at low temperatures (below approximately 298 K), the distances for repressurization *L* are longer at p_{saf} (scenario A) than at 8.5 MPa (scenario B). Nevertheless, between ≅298 and 304 K, the trend progressively reverses for pure CO_2 and for the mixtures with $x_{\mathrm{CO_2}} = 0.9931$, 0.9698, and 0.9532. For the co-capture mixture at 293.15 K, *L* is 433.4 km in scenario A and 368.0 km in B; at 304.21 K, the distances in scenarios A and B are 332.7 km and 346.1 km, respectively.

Figure 7 presents the estimated booster power needed to repressurize the fluid up to a booster outlet pressure of p_{out} = 20.00 MPa, W_{20}, versus the booster inlet temperature, T_{in}. It was assumed that T_{in} coincides with the transport temperature, T_{tr}, and that the outlet temperature, T_{out}, is 38°C (311 K).[66,74,77-79] The considered inlet pressure and density were those given by each of the above presented scenarios: either $p_{\mathrm{in}} = p_{\mathrm{saf}}$ and $\rho_{\mathrm{in}} = \rho_{\mathrm{saf}}$ (scenario A) or $p_{\mathrm{in}} =$

8.50 MPa and $\rho_{\text{in}} = \rho_{8.50\ \text{MPa}}$ (scenario B). The booster efficiency was assumed to be 75%.[74] In scenario A, W_{20} decreases with increasing temperature. It also decreases with increasing SO_2 mole fraction for temperatures up to ≅295 K, but this trend reverses at higher temperatures. In scenario B, W_{20} increases with increasing temperature and decreasing SO_2 concentration.

Below ≅298 K, W_{20} is always lower in scenario B than in A; between ≅298 and 304 K, the trend reverses progressively for pure CO_2 and for the mixtures with $x_{CO_2} = 0.9931$, 0.9698, and 0.9532.

In scenario A, the repressurization distances are always longer for the mixtures than for pure CO_2 in the studied range of temperatures. Conversely, compared to pure CO_2, the needed booster power is lower for the mixtures at temperatures below approximately 295 K but is higher at higher temperatures.

In scenario B, under all the studied conditions, the repressurization distances are longer for the mixtures than for pure CO_2, and the booster powers are lower.

For the co-capture mixture ($x_{CO_2} = 0.9532$) at 293.15 K, repressurization must be performed at L = 433.4 km in scenario A and L = 368.0 km in scenario B compared to 405.2 and 354.9 km, respectively, for pure CO_2. The booster power needed is W_{20} = 6.68 MW in scenario A and W_{20} = 5.52 MW in scenario B for the mixture compared to 6.79 MW and 5.77 MW, respectively, for pure CO_2.

3.3.4. Pipeline inner diameter, *D*. Figures 8, S8 and S9 show the inner diameter of a pipeline, *D*, versus its capacity (mass flow, *m*) for the mixtures and pure CO_2 at the studied compositions and temperatures and at pressures of 8.50, 15.00, and 20.00 MPa. The capacity in the Figures ranges from 310 to 324 kg·s^{-1}, an interval centered on the value used above for *m*: 317.1 kg·s^{-1} = 10 Mt/year. Diameters were iteratively calculated for each mass flow, repeating the calculation

process until the difference between two successive runs was less than 0.1 mm. An average pressure drop per meter of 30 $Pa \cdot m^{-1}$ and a roughness height of the pipeline of 4.6×10^{-5} m were assumed.[52,73]

The inner diameter needed to transport a given mass flow of fluid is lower for the mixtures than for pure CO_2 because of their density and viscosity values, indicating the favorability of the transport of mixtures. The difference increases with increasing concentration of SO_2 and temperature and decreasing pressure. For the co-capture mixture, the inner diameter needed for a flow of 317.1 $kg \cdot s^{-1}$ at 15.00 MPa ranges from 0.499 to 0.517 m within the studied interval of temperatures. For pure CO_2 under the same conditions, the diameters vary between 0.502 and 0.522 m. At 293.15 K and 15.00 MPa, the inner diameter needed to transport 317.1 $kg \cdot s^{-1}$ of the co-capture mixture is 4 mm lower than that for pure CO_2. For a pipeline made of standard carbon steel, API 5L X70, with an inner diameter of 511 mm and a wall thickness of 16.5 mm,[13] this difference in inner diameter corresponds to a reduction of approximately 840 kg of steel per km of pipeline.

3.4. Joule-Thomson Coefficient, μ_{JT}. Figures 9 and S10 show the $\mu_{JT} - p$ isotherms for the studied CO_2+SO_2 mixtures and pure CO_2 at 273.15, 293.15 and 304.21 K. The calculations at 263.15 K were not addressed due to the lack of the required experimental values at lower temperatures. In this section, composition is given as mole fraction of SO_2, x_{SO_2}, because in the calculations of μ_{JT}, we used densities measured in binary CO_2+SO_2 mixtures and speeds of sound determined in both binary CO_2+SO_2 and ternary (doped) CO_2+CH_3OH+SO_2 mixtures. The mole fraction of SO_2 in the respective binary and ternary mixtures is the same. μ_{JT} is lower for the mixtures than for pure CO_2 at each temperature. At a given temperature, μ_{JT} (CO_2) −

μ_{JT}(mixture) increases with increasing concentration of SO_2 in the mixture. For a given concentration of SO_2, μ_{JT} $(CO_2) - \mu_{JT}$(mixture) increases with increasing temperature.

At 293.15 and 304.21 K, μ_{JT} is positive for all the studied compositions and pressures, and the fluid cools under depressurization. At 273.15 K, the four most SO_2-rich mixtures, i.e., $x_{SO_2} =$ 0.1971, 0.1031, 0.0468, and 0.0302, exhibited experimental inversion pressures (cooling-warming change) of 10.8, 16.1, 19.6 and 20.3 MPa, respectively, which are the pressures below which the coefficients are positive and above which they are negative. Extrapolation of the results for the $x_{SO_2} = 0.0069$ mixture provides an inversion pressure of 21.6 MPa.

Figures 9 and S10 also include the values of μ_{JT} calculated with the extended EOS-CG and the PC-SAFT EoS for the mixtures and those found in the literature for pure CO_2.[55] Table S11 presents for each isotherm the deviations between the experimental values and those calculated using the respective EoS in terms of the average absolute deviation, $\overline{AAD}_{\mu_{JT}}$. The global average values of the deviations were 0.025 K·MPa^{-1} for extended EOS-CG and 0.027 K·MPa^{-1} for PC-SAFT.

Figure 10 shows the inversion line for pure CO_2[55] and the inversion pressures at 273.15 K for the five mixtures. The presence of SO_2 shifts the inversion points to lower pressures: the higher the SO_2 concentration, the lower the inversion pressure. Figure 11 presents the inversion pressures at 273.15 K as a function of the SO_2 mole fraction, showing a good linear correlation.

4. CONCLUSIONS

Some authors proposed that the presence of SO_2 in the stream could favor some steps of CCS technology and thus proposed CO_2/SO_2 co-capture. To assess this possibility, we determined the impact of the presence of SO_2 on several transport parameters and on the Joule-Thomson coefficient, which are required for the safety and profitability of CCS technology. For this

purpose, we determined the densities and vapor-liquid equilibria data of five CO_2-rich CO_2+SO_2 mixtures under conditions which include those of interest for CCS: $0.80 \leq x_{CO_2} \leq 0.99$, $263.15 \leq T \leq 304.21$ K, and pressures up to 20 MPa. Similarly, we determined the speeds of sound for four of these mixtures at the same temperatures and at pressures up to 190 MPa (the speed of sound of the remaining mixture was previously published). For the *c* measurements, the mixtures with $x_{CO_2} > 0.90$ were doped with ≅0.8 mole % of methanol to obtain proper signals. Suitable polynomials were fitted to the experimental results for the speed of sound and extrapolated to the low-pressure zone, where despite the doping, no signals were detected. The combined uncertainties obtained for the experimental results were as follows: average $u_\rho = 0.49$ kg·m^{-3}; average $u_{p_d,p_b} = 0.017$ MPa; average $u_{\rho_V,\rho_L} = 1.05$ kg·m^{-3}; $u_c = 6.2 \times 10^{-4} c$ for CO_2+SO_2 and $u_c = 8.1 \times 10^{-4} c$ for CO_2+CH_3OH+SO_2. Only one reference with volumetric data for the studied mixtures and conditions was found in the literature, which is in good agreement with our results. Three original references were found on vapor-liquid equilibrium, most of them in good agreement with our results. No data were found on speed of sound of the studied systems.

The mixtures were modeled using the extended EOS-CG model as implemented in TREND 2.0.1. and the PC-SAFT equation of state. From the obtained deviations, we concluded that PC-SAFT with the parameters shown in Table S8, and extended EOS-CG properly reproduce the measured properties of the CO_2+SO_2 system under these operating conditions, which include those of interest for CCS. The extended EOS-CG reproduces the speed of sound better than the PC-SAFT EoS. However, extended EOS-CG provides anomalous predictions for the density of the phases at equilibrium for the most CO_2-rich mixture under conditions near its critical point. By comparing the extrapolated *c* values with those obtained with both equations of state, we validated our extrapolated results for the speed of sound.

Using our experimental data and viscosities from literature, we calculated selected parameters related to the transport of the studied CO_2+SO_2 mixtures by pipeline and compared them with those determined for pure CO_2 to assess the convenience of transport CO_2 containing SO_2. We found that the presence of SO_2 favors some aspects of the transport step compared to pure CO_2: it reduces the minimum operational pressure, the pressure and density drops along the pipeline, and the inner diameter needed to transport a given mass flow, and it increases the distance allowed between boosters at all the studied pressures and temperatures. The needed booster power for repressurization is lower for the mixtures than for pure CO_2 at all the studied compositions and temperatures when the repressurization is conducted at a minimum pressure of 8.50 MPa (scenario B). The scenario A considered in this work consists in repressurizing when the density of the fluid reaches a minimum value of 800 $kg \cdot m^{-3}$, always keeping a minimum safety margin of 1 MPa above the bubble pressure. In scenario A, the booster power for the mixtures is lower than that for pure CO_2 below approximately 295 K but becomes higher at higher temperatures. At low temperatures, repressurization in scenario A enables longer distances between boosters than repressurization at 8.50 MPa, but it demands higher booster power; at high temperatures, the opposite behavior is observed. Regarding the repressurization distance, scenario A is clearly more sensitive to composition and temperature than scenario B.

We calculated the Joule-Thomson coefficients of the mixtures at 273.15, 293.15 and 304.21 K. These values were lower than those for pure CO_2, leading to a lower cooling of the anthropogenic CO_2 containing SO_2 during expansion. The differences increase with increasing SO_2 concentration and temperature. At 293.15 and 304.21 K, the obtained μ_{JT} values were positive, which indicates fluid cooling under expansion. At 273.15 K, the experimental inversion

pressures of the mixtures were in the range from 10.8 to 21.6 MPa, and the higher the SO_2 concentration, the lower the inversion pressure.

At 293.15 K, a mixture containing 5 mole % of SO_2 presents, a reduction of 6.1% in the minimum transport pressure compared to pure CO_2 if repressurizations are accomplished 1 MPa over their respective p_{bubble}. For this case and the pipeline considered in this work, the pressure and density drops at 300 km reduce by 1.6%. Moreover, the distance between boosters decreases by 6.9% and 3.7% in scenarios A and B respectively, and the booster power reduces by 1.6% and 4.0%, respectively. In addition, the requirement of a lower diameter leads to a reduction of 840 kg of steel per km of pipeline. Finally, the Joule-Thomson coefficients for this co-capture mixture show reductions up to 35% over the studied ranges of T and p, resulting in less cooling during expansion.

Authors concluded in a previous paper that the impact of SO_2 on hydraulic and thermodynamic aspects of injection and storage is also beneficial. The conclusions of both works would indicate that CO_2/SO_2 co-capture may be a viable technology to lower the costs in CCS and to mitigate the emission of SO_2 to the atmosphere. Nevertheless the possibility of corrosion, induced geochemical reactions, and risks associated with potential leakage from the pipeline network or the storage reservoirs were not included in our studies. The global conclusions must be derived from the balance of technical, economic and safety factors, as well as environmental considerations.

TABLES

Table 1. $p\rho T x_{CO_2}$ experimental data for the CO_2+SO_2 mixtures. u_ρ: combined uncertainty.

$x_{CO_2} = 0.8029$											
T=263.15±0.05 K			T=273.15±0.05 K			T=293.15±0.05 K			T=304.21±0.05 K		
p (MPa)	ρ (kg·m^{-3})	u_ρ (kg·m^{-3})	p (MPa)	ρ (kg·m^{-3})	u_ρ (kg·m^{-3})	p (MPa)	ρ (kg·m^{-3})	u_ρ (kg·m^{-3})	p (MPa)	ρ (kg·m^{-3})	u_ρ (kg·m^{-3})
0.100	2.50	0.24	0.100	1,5	0.23	0.100	2.11	0.24	0.100	1.86	0.23
0.156	3.82	0.24	0.182	4.03	0.23	0.230	4.68	0.24	0.277	5.16	0.23
0.212	5.10	0.23	0.263	5.86	0.23	0.361	7.36	0.24	0.454	8.65	0.23
0.268	6.36	0.23	0.345	7.65	0.23	0.491	10.06	0.24	0.630	12.21	0.23
0.323	7.62	0.23	0.427	9.49	0.23	0.621	12.82	0.24	0.807	15.91	0.23
0.379	8.98	0.23	0.508	11.34	0.23	0.751	15.60	0.24	0.984	19.63	0.23
0.435	10.40	0.23	0.590	13.26	0.23	0.882	18.54	0.24	1.161	23.40	0.23
0.491	11.72	0.23	0.672	15.21	0.23	1.012	21.48	0.24	1.338	27.40	0.24
2.134	1101.18	0.61	0.767	17.46	0.22	1.142	24.45	0.24	1.515	31.45	0.24
2.569	1102.93	0.61	3.013	1059.70	0.59	1.273	27.55	0.24	1.691	35.59	0.24
3.005	1104.57	0.61	3.447	1061.84	0.59	1.403	30.81	0.24	1.868	39.83	0.24
3.441	1106.25	0.61	3.881	1064.00	0.59	1.631	36.49	0.24	2.045	44.26	0.24
3.877	1107.88	0.61	4.315	1066.17	0.59	4.395	972.88	1.87	2.222	48.77	0.24
4.312	1109.54	0.61	4.750	1068.26	0.59	4.821	977.32	1.64	2.318	51.29	0.24
4.748	1111.09	0.61	5.184	1070.33	0.59	5.247	981.38	1.41	2.415	53.90	0.24
5.184	1112.65	0.61	5.618	1072.34	0.60	5.673	985.19	1.19	5.633	887.53	1.26
5.620	1114.19	0.61	6.052	1074.27	0.60	6.100	988.77	0.56	6.061	894.39	1.11
6.056	1115.76	0.61	6.486	1076.22	0.60	6.526	992.35	0.56	6.490	900.35	0.96
6.491	1117.22	0.62	6.920	1078.10	0.60	6.952	995.71	0.56	6.918	905.87	0.81
6.927	1118.73	0.62	7.355	1079.86	0.60	7.378	998.97	0.56	7.347	910.89	0.70
7.363	1120.17	0.62	7.789	1081.60	0.60	7.804	1002.02	0.57	7.776	915.43	0.54
7.799	1121.50	0.62	8.223	1083.40	0.60	8.231	1005.04	0.57	8.204	919.65	0.54
8.234	1122.94	0.62	8.657	1085.12	0.60	8.657	1008.18	0.57	8.633	924.05	0.54
8.670	1124.39	0.62	9.091	1086.86	0.60	9.083	1011.20	0.57	9.062	928.35	0.54
9.106	1125.82	0.62	9.526	1088.54	0.60	9.509	1014.01	0.57	9.490	932.35	0.54
9.542	1127.20	0.62	9.960	1090.18	0.60	9.935	1016.82	0.57	9.919	936.18	0.54
9.977	1128.49	0.62	10.394	1091.88	0.60	10.362	1019.53	0.57	10.347	939.99	0.54
10.413	1129.84	0.62	10.828	1093.60	0.60	10.788	1022.19	0.57	10.776	943.71	0.54
10.849	1131.15	0.62	11.262	1095.26	0.60	11.214	1024.93	0.57	11.205	947.23	0.54
11.285	1132.49	0.62	11.696	1096.90	0.61	11.640	1027.52	0.57	11.633	950.60	0.54
11.720	1133.79	0.62	12.131	1098.48	0.61	12.066	1030.04	0.58	12.062	953.80	0.54
12.156	1135.07	0.62	12.565	1100.07	0.61	12.492	1032.51	0.58	12.491	956.99	0.54
12.592	1136.38	0.62	12.999	1101.63	0.61	12.919	1034.95	0.58	12.919	960.09	0.54
13.028	1137.61	0.62	13.433	1103.14	0.61	13.345	1037.33	0.58	13.348	963.01	0.54
13.464	1138.86	0.62	13.849	1104.58	0.61	13.771	1039.62	0.58	13.776	965.95	0.55
13.899	1140.11	0.62	14.283	1106.08	0.61	14.197	1041.96	0.58	14.205	968.75	0.55
14.335	1141.34	0.63	14.718	1107.50	0.61	14.623	1044.12	0.58	14.634	971.51	0.55
14.771	1142.57	0.63	15.152	1108.98	0.61	15.050	1046.30	0.58	15.062	974.25	0.55
15.207	1143.78	0.63	15.586	1110.36	0.61	15.476	1048.45	0.58	15.491	976.86	0.55
15.642	1145.02	0.63	16.020	1111.82	0.61	15.902	1050.58	0.58	15.920	979.48	0.55
16.078	1146.19	0.63	16.454	1113.20	0.61	16.328	1052.69	0.58	16.348	981.95	0.55
16.514	1147.40	0.63	16.888	1114.58	0.61	16.754	1054.71	0.59	16.777	984.48	0.55

16.950	1148.56	0.63	17.323	1115.95	0.61	17.181	1056.74	0.59	17.205	986.90	0.55
17.385	1149.69	0.63	17.757	1117.36	0.61	17.607	1058.72	0.59	17.634	989.33	0.55
17.821	1150.85	0.63	18.191	1118.72	0.62	18.033	1060.64	0.59	18.063	991.67	0.56
18.257	1152.01	0.63	18.625	1120.07	0.62	18.459	1062.54	0.59	18.491	993.94	0.56
18.693	1153.10	0.63	19.059	1121.36	0.62	18.885	1064.39	0.59	18.920	996.22	0.56
19.128	1154.25	0.63	19.493	1122.69	0.62	19.312	1066.20	0.59	19.348	998.52	0.56
19.564	1155.32	0.63	19.928	1123.99	0.62	19.738	1068.04	0.59	19.777	1000.79	0.56
20.000	1156.42	0.63	20.000	1124.19	0.62	20.000	1069.11	0.59	20.000	1001.87	0.56

Table 1 (continued). $p\rho T x_{CO_2}$ experimental data for the CO_2+SO_2 mixtures. u_ρ: combined uncertainty.

$x_{CO_2} = 0.8969$											
T=263.15±0.05 K			T=273.15±0.05 K			T=293.15±0.05 K			T=304.21±0.05 K		
p (MPa)	ρ (kg·m^{-3})	u_ρ (kg·m^{-3})	p (MPa)	ρ (kg·m^{-3})	u_ρ (kg·m^{-3})	p (MPa)	ρ (kg·m^{-3})	u_ρ (kg·m^{-3})	p (MPa)	ρ (kg·m^{-3})	u_ρ (kg·m^{-3})
0.100	2.43	0.24	0.107	2.37	0.23	0.100	1.89	0.23	0.100	1.95	0.24
0.214	4.95	0.23	0.239	5.14	0.23	0.362	7.22	0.23	0.394	7.61	0.23
0.328	7.49	0.23	0.371	7.91	0.23	0.624	12.67	0.23	0.687	13.34	0.23
0.442	10.16	0.23	0.489	10.44	0.23	0.886	18.20	0.23	0.981	19.41	0.23
0.557	12.84	0.23	0.655	14.08	0.23	1.148	23.73	0.23	1.274	25.73	0.23
0.671	15.59	0.23	0.796	17.24	0.23	1.410	29.66	0.23	1.568	32.29	0.24
0.785	18.38	0.23	0.919	20.09	0.23	1.671	35.81	0.23	1.861	39.21	0.24
0.866	20.67	0.23	1.115	24.84	0.23	1.933	42.18	0.23	2.155	46.53	0.24
2.512	1057.15	0.58	1.293	29.12	0.23	2.195	48.75	0.23	2.449	54.23	0.24
2.954	1059.28	0.59	3.319	1005.14	0.56	2.457	55.53	0.23	2.742	62.22	0.24
3.397	1061.16	0.59	3.748	1008.36	0.56	2.719	62.75	0.23	3.036	70.27	0.24
3.839	1063.04	0.59	4.182	1011.18	0.56	2.865	66.92	0.23	3.329	78.32	0.24
4.281	1064.84	0.59	4.616	1013.84	0.56	5.107	895.64	1.30	3.623	86.69	0.24
4.723	1066.66	0.59	5.050	1016.54	0.57	5.514	900.68	1.16	3.917	95.47	0.24
5.166	1068.48	0.59	5.483	1019.06	0.57	5.929	906.25	0.52	4.126	102.16	0.24
5.608	1070.15	0.59	5.917	1021.49	0.57	6.343	911.11	0.52	6.199	795.76	0.93
6.050	1071.83	0.59	6.351	1023.94	0.57	6.741	915.24	0.52	6.617	808.73	0.88
6.492	1073.53	0.59	6.785	1026.36	0.57	7.155	919.56	0.52	7.035	819.52	0.76
6.935	1075.13	0.59	7.219	1028.71	0.57	7.570	923.61	0.52	7.454	829.05	0.50
7.377	1076.72	0.59	7.653	1031.11	0.57	7.984	927.48	0.53	7.872	837.18	0.50
7.819	1078.39	0.59	8.087	1033.33	0.57	8.398	931.33	0.53	8.290	844.72	0.50
8.261	1079.94	0.59	8.521	1035.52	0.57	8.813	934.97	0.53	8.708	851.59	0.50
8.704	1081.51	0.60	8.954	1037.69	0.58	9.227	938.50	0.53	9.126	858.03	0.50
9.146	1083.04	0.60	9.388	1039.81	0.58	9.641	941.91	0.53	9.545	863.92	0.50
9.588	1084.49	0.60	9.822	1041.84	0.58	10.056	945.29	0.53	9.963	869.50	0.50
10.031	1085.99	0.60	10.256	1043.86	0.58	10.470	948.52	0.53	10.381	874.78	0.50
10.473	1087.44	0.60	10.690	1045.82	0.58	10.884	951.56	0.54	10.799	879.77	0.51
10.915	1088.90	0.60	11.124	1047.82	0.58	11.299	954.42	0.54	11.218	884.47	0.51
11.357	1090.33	0.60	11.558	1049.79	0.58	11.713	957.27	0.54	11.636	888.93	0.51
11.800	1091.75	0.60	11.991	1051.68	0.58	12.127	960.07	0.54	12.054	893.21	0.51
12.242	1093.18	0.60	12.425	1053.63	0.58	12.542	962.78	0.54	12.472	897.43	0.51
12.684	1094.58	0.60	12.859	1055.44	0.58	12.956	965.47	0.54	12.890	901.43	0.51
13.126	1095.90	0.60	13.293	1057.17	0.58	13.370	968.14	0.54	13.309	905.29	0.51
13.569	1097.27	0.60	13.727	1058.97	0.58	13.785	970.76	0.54	13.727	909.03	0.52

14.011	1098.54	0.60	14.161	1060.71	0.59	14.199	973.33	0.54	14.145	912.64	0.52
14.453	1099.88	0.60	14.595	1062.50	0.59	14.613	975.86	0.55	14.563	916.07	0.52
14.895	1101.16	0.60	15.029	1064.23	0.59	15.028	978.30	0.55	14.981	919.39	0.52
15.338	1102.49	0.60	15.462	1065.98	0.59	15.442	980.70	0.55	15.400	922.65	0.52
15.780	1103.73	0.61	15.896	1067.65	0.59	15.857	983.01	0.55	15.818	925.86	0.52
16.222	1105.05	0.61	16.330	1069.37	0.59	16.271	985.34	0.55	16.236	928.98	0.52
16.665	1106.33	0.61	16.764	1071.00	0.59	16.685	987.52	0.55	16.654	931.99	0.53
17.107	1107.47	0.61	17.198	1072.70	0.59	17.100	989.59	0.55	17.073	934.97	0.53
17.549	1108.71	0.61	17.632	1074.27	0.59	17.514	991.77	0.55	17.491	937.86	0.53
17.991	1109.94	0.61	18.066	1075.88	0.59	17.928	993.86	0.55	17.909	940.68	0.53
18.434	1111.09	0.61	18.500	1077.45	0.59	18.343	995.82	0.55	18.327	943.38	0.53
18.876	1112.25	0.61	18.933	1078.95	0.59	18.757	997.95	0.55	18.745	946.05	0.53
19.318	1113.38	0.61	19.367	1080.49	0.59	19.171	999.97	0.56	19.164	948.69	0.53
19.760	1114.51	0.61	19.801	1081.96	0.59	19.586	1001.95	0.56	19.582	951.15	0.53
19.871	1114.83	0.61	19.928	1082.39	0.59	19.785	1002.93	0.56	19.808	952.43	0.53
20.000	1115.11	0.61	20.000	1082.61	0.59	20.000	1003.92	0.56	20.000	953.37	0.53

Table 1 (continued). $p\rho T x_{CO_2}$ experimental data for the CO_2+SO_2 mixtures. u_ρ: combined uncertainty.

x_{CO_2} = 0.9532											
T=263.15±0.05 K			T=273.15±0.05 K			T=293.15±0.05 K			T=304.21±0.05 K		
p (MPa)	ρ (kg·m^{-3})	u_ρ (kg·m^{-3})	p (MPa)	ρ (kg·m^{-3})	u_ρ (kg·m^{-3})	p (MPa)	ρ (kg·m^{-3})	u_ρ (kg·m^{-3})	p (MPa)	ρ (kg·m^{-3})	u_ρ (kg·m^{-3})
0.100	2.43	0.25	0.100	2.27	0.24	0.100	2.01	0.24	0.100	1.80	0.23
0.300	6.69	0.23	0.358	7.55	0.23	0.501	9.78	0.24	0.512	9.49	0.23
0.499	11.10	0.23	0.616	13.05	0.23	0.881	17.45	0.24	0.924	17.34	0.23
0.699	15.67	0.23	0.897	19.30	0.23	1.261	25.57	0.23	1.336	25.76	0.23
0.898	20.55	0.23	1.178	25.89	0.23	1.641	34.03	0.24	1.747	34.69	0.23
1.098	25.52	0.23	1.436	32.24	0.23	2.021	43.02	0.23	2.159	44.06	0.23
1.328	31.57	0.23	1.694	38.92	0.23	2.401	52.62	0.23	2.571	53.90	0.23
1.559	38.28	0.23	1.952	45.98	0.23	2.780	62.90	0.23	2.983	64.18	0.23
2.718	1018.24	0.39	2.280	55.72	0.23	3.160	74.19	0.23	3.395	75.40	0.23
3.142	1020.89	0.39	3.620	968.41	0.38	3.540	86.56	0.23	3.807	87.54	0.23
3.586	1023.20	0.39	4.042	971.45	0.38	3.920	100.50	0.23	4.218	100.94	0.24
4.010	1025.43	0.39	4.464	974.26	0.38	4.300	116.65	0.23	4.630	116.02	0.24
4.454	1027.67	0.39	4.886	977.42	0.38	5.330	828.42	1.09	5.042	133.28	0.24
4.878	1029.71	0.39	5.308	980.07	0.38	5.731	837.31	0.35	5.454	153.59	0.25
5.322	1031.78	0.39	5.729	982.81	0.38	6.134	844.79	0.35	5.895	181.21	0.26
5.746	1033.79	0.39	6.133	985.40	0.38	6.537	851.68	0.35	6.748	722.45	0.68
6.190	1035.75	0.39	6.537	987.87	0.38	6.940	857.73	0.35	7.146	744.47	0.58
6.614	1037.67	0.39	6.958	990.41	0.38	7.343	863.48	0.35	7.545	760.68	0.46
7.058	1039.63	0.39	7.380	992.83	0.38	7.746	868.95	0.35	7.943	772.96	0.46
7.482	1041.51	0.39	7.802	995.27	0.38	8.149	874.06	0.35	8.342	784.45	0.46
7.926	1043.40	0.39	8.224	997.59	0.38	8.552	878.82	0.36	8.740	794.48	0.47
8.350	1045.22	0.39	8.646	999.87	0.38	8.955	883.43	0.36	9.139	803.35	0.47
8.794	1047.08	0.39	9.068	1002.07	0.38	9.358	887.75	0.36	9.538	811.29	0.47
9.218	1048.79	0.40	9.490	1004.27	0.38	9.761	891.86	0.36	9.936	818.56	0.48
9.662	1050.58	0.40	9.912	1006.45	0.39	10.164	895.73	0.36	10.335	825.37	0.48
10.105	1052.35	0.40	10.333	1008.50	0.39	10.567	899.57	0.36	10.733	831.77	0.48

10.530	1054.02	0.40	10.755	1010.62	0.39	10.970	903.27	0.36	11.132	837.66	0.48
10.973	1055.73	0.40	11.177	1012.66	0.39	11.373	906.90	0.36	11.530	843.35	0.49
11.398	1057.36	0.40	11.599	1014.64	0.39	11.776	910.39	0.36	11.929	848.64	0.49
11.841	1059.03	0.40	12.021	1016.62	0.39	12.179	913.70	0.36	12.311	853.52	0.49
12.285	1060.68	0.40	12.443	1018.59	0.39	12.582	916.99	0.36	12.710	858.34	0.49
12.709	1062.24	0.40	12.846	1020.39	0.39	12.985	920.11	0.36	13.108	863.01	0.49
13.153	1063.81	0.40	13.268	1022.23	0.39	13.388	923.19	0.36	13.507	867.42	0.50
13.577	1065.40	0.40	13.690	1024.09	0.39	13.791	926.19	0.37	13.905	871.71	0.50
14.021	1066.97	0.40	14.112	1025.91	0.39	14.194	929.13	0.37	14.304	875.78	0.50
14.445	1068.49	0.40	14.516	1027.65	0.39	14.597	932.06	0.37	14.702	879.77	0.50
14.889	1070.03	0.40	14.937	1029.39	0.39	15.000	934.91	0.37	15.101	883.54	0.50
15.332	1071.58	0.40	15.359	1031.10	0.39	15.403	937.58	0.37	15.500	887.27	0.50
15.757	1072.96	0.40	15.781	1032.81	0.39	15.806	940.29	0.37	15.898	890.86	0.51
16.200	1074.52	0.40	16.203	1034.52	0.39	16.208	942.90	0.37	16.297	894.36	0.51
16.625	1075.88	0.40	16.625	1036.19	0.39	16.611	945.47	0.37	16.695	897.70	0.51
17.068	1077.36	0.40	17.047	1037.84	0.39	16.996	947.88	0.37	17.094	900.90	0.51
17.512	1078.79	0.40	17.469	1039.49	0.39	17.399	950.24	0.37	17.492	904.06	0.51
17.936	1080.17	0.40	17.891	1041.08	0.39	17.802	952.71	0.37	17.891	907.13	0.51
18.303	1081.29	0.40	18.312	1042.66	0.39	18.205	955.03	0.37	18.289	910.09	0.51
18.843	1082.95	0.40	18.808	1044.53	0.39	18.608	957.33	0.37	18.688	912.96	0.51
19.190	1083.98	0.40	19.120	1045.65	0.39	19.011	959.56	0.37	19.087	915.88	0.52
19.441	1084.73	0.40	19.395	1046.63	0.39	19.304	961.14	0.37	19.485	918.63	0.52
19.730	1085.56	0.40	19.670	1047.58	0.39	19.707	963.33	0.37	19.768	920.49	0.52
20.000	1086.34	0.40	20.000	1048.75	0.39	20.000	964.83	0.37	20.000	922.01	0.52

Table 1 (continued). $p\rho T x_{CO_2}$ experimental data for the CO_2+SO_2 mixtures. u_ρ: combined uncertainty.

x_{CO_2} = 0.9698											
T=263.15±0.05 K			T=273.15±0.05 K			T=293.15±0.05 K			T=304.21±0.05 K		
p (MPa)	ρ (kg·m^{-3})	u_ρ (kg·m^{-3})	p (MPa)	ρ (kg·m^{-3})	u_ρ (kg·m^{-3})	p (MPa)	ρ (kg·m^{-3})	u_ρ (kg·m^{-3})	p (MPa)	ρ (kg·m^{-3})	u_ρ (kg·m^{-3})
0.100	2.43	0.25	0.100	2.11	0.23	0.100	2.16	0.25	0.100	1.99	0.24
0.356	7.81	0.23	0.417	8.53	0.23	0.526	10.21	0.23	0.544	9.92	0.23
0.612	13.48	0.23	0.733	15.27	0.23	0.952	19.04	0.23	0.989	18.41	0.23
0.869	19.37	0.23	1.050	22.72	0.23	1.378	27.96	0.23	1.433	27.47	0.23
1.125	25.59	0.23	1.366	30.02	0.23	1.803	37.58	0.23	1.877	36.97	0.23
1.381	32.25	0.23	1.683	38.12	0.23	2.253	48.33	0.23	2.322	46.90	0.23
1.617	38.86	0.23	2.000	46.78	0.23	2.702	60.00	0.23	2.766	57.54	0.23
1.913	48.13	0.23	2.316	56.70	0.23	3.128	72.09	0.23	3.242	69.74	0.23
2.701	1007.43	0.56	2.581	65.83	0.23	3.554	85.57	0.23	3.718	83.15	0.23
3.125	1009.66	0.56	3.916	958.46	0.54	3.980	100.64	0.23	4.163	96.93	0.23
3.549	1011.82	0.56	4.794	965.62	0.54	4.406	118.36	0.23	4.607	112.20	0.24
3.973	1014.04	0.56	5.197	968.52	0.54	4.822	139.27	0.24	5.051	129.78	0.24
4.396	1016.24	0.56	5.581	971.30	0.54	5.479	816.46	1.01	5.496	150.15	0.24
4.820	1018.42	0.56	5.965	973.96	0.54	5.882	824.86	0.34	5.940	174.86	0.25
5.244	1020.52	0.56	6.368	976.53	0.54	6.284	833.40	0.35	6.384	209.86	0.26
5.668	1022.57	0.56	6.752	978.87	0.54	6.686	840.37	0.35	7.708	734.63	0.44
6.092	1024.61	0.57	7.136	981.17	0.55	7.089	847.14	0.35	8.068	747.17	0.45
6.515	1026.57	0.57	7.521	983.48	0.55	7.491	853.33	0.35	8.444	759.88	0.45

6.939	1028.52	0.57	7.905	985.81	0.55	7.893	859.19	0.35	8.804	769.91	0.45
7.363	1030.45	0.57	8.289	988.07	0.55	8.296	864.71	0.35	9.181	779.63	0.46
7.787	1032.33	0.57	8.692	990.36	0.55	8.698	869.93	0.35	9.541	787.56	0.46
8.191	1034.10	0.57	9.094	992.62	0.55	9.100	874.79	0.35	9.917	794.81	0.46
8.615	1035.94	0.57	9.497	994.83	0.55	9.503	879.30	0.35	10.277	801.89	0.47
9.039	1037.70	0.57	9.899	996.97	0.55	9.905	883.66	0.36	10.654	808.58	0.47
9.463	1039.49	0.57	10.302	999.07	0.55	10.307	887.80	0.36	11.014	814.77	0.47
9.887	1041.21	0.57	10.705	1001.08	0.55	10.710	891.81	0.36	11.390	820.60	0.47
10.310	1042.94	0.57	11.107	1003.18	0.56	11.112	895.68	0.36	11.751	825.96	0.48
10.734	1044.63	0.57	11.510	1005.15	0.56	11.514	899.41	0.36	12.127	831.10	0.48
11.158	1046.27	0.57	11.912	1007.13	0.56	11.917	903.08	0.36	12.487	835.86	0.48
11.582	1047.98	0.58	12.315	1009.07	0.56	12.319	906.61	0.36	12.864	840.64	0.48
12.006	1049.56	0.58	12.717	1010.99	0.56	12.721	910.04	0.36	13.224	845.05	0.48
12.429	1051.16	0.58	13.120	1012.94	0.56	13.124	913.41	0.36	13.600	849.33	0.49
12.853	1052.79	0.58	13.522	1014.82	0.56	13.526	916.65	0.36	13.960	853.41	0.49
13.277	1054.34	0.58	13.925	1016.59	0.56	13.928	919.83	0.36	14.337	857.52	0.49
13.701	1055.89	0.58	14.328	1018.47	0.56	14.331	922.88	0.36	14.713	861.47	0.49
14.125	1057.43	0.58	14.730	1020.20	0.56	14.733	925.87	0.36	15.073	865.14	0.49
14.548	1058.92	0.58	15.133	1022.02	0.56	15.135	928.75	0.37	15.450	868.81	0.49
14.972	1060.44	0.58	15.535	1023.67	0.57	15.538	931.58	0.37	15.810	872.24	0.50
15.396	1062.00	0.58	15.938	1025.43	0.57	15.940	934.34	0.37	16.186	875.70	0.50
15.820	1063.43	0.58	16.340	1027.07	0.57	16.342	936.95	0.37	16.546	878.89	0.50
16.244	1064.87	0.58	16.743	1028.75	0.57	16.745	939.54	0.37	16.923	882.21	0.50
16.667	1066.34	0.58	17.145	1030.36	0.57	17.147	942.02	0.37	17.283	885.25	0.50
17.091	1067.71	0.58	17.548	1032.00	0.57	17.549	944.46	0.37	17.659	888.26	0.50
17.515	1069.09	0.59	17.951	1033.61	0.57	17.952	946.80	0.37	18.019	891.19	0.50
17.939	1070.48	0.59	18.353	1035.15	0.57	18.354	949.14	0.37	18.396	894.13	0.51
18.363	1071.82	0.59	18.756	1036.68	0.57	18.756	951.35	0.37	18.756	896.76	0.51
18.786	1073.17	0.59	19.103	1038.04	0.57	19.122	953.27	0.37	19.083	899.25	0.51
19.210	1074.48	0.59	19.396	1039.14	0.57	19.433	954.94	0.37	19.427	901.72	0.51
19.634	1075.81	0.59	19.744	1040.42	0.57	19.726	956.34	0.37	19.722	903.72	0.51
20.000	1076.87	0.59	20.000	1041.34	0.57	20.000	957.70	0.37	20.000	905.60	0.51

Table 1 (continued). $p\rho T x_{CO_2}$ experimental data for the CO_2+SO_2 mixtures. u_ρ: combined uncertainty.

$x_{CO_2} = 0.9931$											
T=263.15±0.05 K			T=273.15±0.05 K			T=293.15±0.05 K			T=304.21±0.05 K		
p (MPa)	ρ (kg·m^{-3})	u_ρ (kg·m^{-3})	p (MPa)	ρ (kg·m^{-3})	u_ρ (kg·m^{-3})	p (MPa)	ρ (kg·m^{-3})	u_ρ (kg·m^{-3})	p (MPa)	ρ (kg·m^{-3})	u_ρ (kg·m^{-3})
0.100	2.41	0.25	0.100	1.95	0.22	0.100	1.81	0.22	0.100	1.72	0.22
0.406	8.90	0.23	0.470	9.43	0.22	0.615	11.59	0.22	0.568	10.17	0.22
0.712	15.68	0.23	0.861	17.83	0.22	1.130	21.86	0.22	1.035	19.06	0.22
1.018	22.92	0.23	1.252	26.74	0.22	1.618	32.30	0.22	1.503	28.34	0.22
1.324	30.58	0.23	1.622	35.81	0.23	2.106	43.71	0.23	1.971	38.23	0.23
1.630	38.75	0.23	2.014	46.20	0.23	2.675	57.74	0.23	2.438	48.68	0.23
1.936	47.65	0.23	2.405	57.67	0.23	3.136	70.56	0.23	2.906	59.79	0.23
2.242	57.59	0.23	2.818	71.30	0.23	3.488	81.12	0.23	3.374	71.85	0.23
2.788	988.48	0.55	3.290	89.81	0.23	3.895	94.56	0.23	3.841	84.86	0.23
3.211	992.02	0.55	3.608	934.02	0.52	4.328	110.74	0.23	4.309	99.24	0.23

3.634	994.55	0.55	4.015	937.75	0.52	4.898	136.45	0.24	4.777	115.18	0.23
4.057	997.02	0.55	4.440	940.79	0.53	5.494	174.06	0.24	5.244	133.51	0.24
4.480	999.40	0.55	4.866	944.42	0.53	5.726	787.14	0.91	5.712	154.91	0.24
4.903	1001.66	0.55	5.292	947.74	0.53	6.120	796.99	0.46	6.290	188.48	0.25
5.307	1003.80	0.55	5.718	950.87	0.53	6.514	806.65	0.47	6.958	250.74	0.26
5.730	1006.04	0.56	6.143	953.89	0.53	6.908	815.22	0.47	8.149	711.65	0.44
6.153	1008.20	0.56	6.569	956.81	0.53	7.302	822.50	0.47	8.354	722.16	0.44
6.577	1010.33	0.56	6.995	959.73	0.53	7.696	829.61	0.48	8.728	736.08	0.44
7.000	1012.43	0.56	7.421	962.56	0.54	8.090	836.37	0.48	9.174	748.97	0.44
7.403	1014.33	0.56	7.846	965.35	0.54	8.484	842.04	0.48	9.529	759.15	0.45
7.827	1016.39	0.56	8.272	968.06	0.54	8.878	847.70	0.48	9.883	768.37	0.45
8.250	1018.40	0.56	8.698	970.64	0.54	9.272	852.96	0.49	10.238	776.48	0.45
8.673	1020.37	0.56	9.104	973.03	0.54	9.666	858.07	0.49	10.593	784.19	0.46
9.096	1022.21	0.56	9.530	975.47	0.54	10.060	862.77	0.49	10.947	791.11	0.46
9.519	1024.10	0.56	9.956	977.78	0.54	10.454	867.10	0.49	11.302	797.53	0.46
9.942	1025.97	0.56	10.382	980.13	0.54	10.848	871.28	0.49	11.657	803.31	0.46
10.365	1027.75	0.57	10.807	982.46	0.54	11.242	875.44	0.50	12.011	809.06	0.47
10.788	1029.56	0.57	11.233	984.78	0.55	11.636	879.41	0.50	12.366	814.51	0.47
11.211	1031.23	0.57	11.659	986.95	0.55	12.030	883.07	0.50	12.721	819.51	0.47
11.634	1032.95	0.57	12.085	989.14	0.55	12.424	886.61	0.50	13.075	824.13	0.47
12.057	1034.75	0.57	12.510	991.26	0.55	12.818	890.28	0.50	13.430	828.67	0.48
12.481	1036.38	0.57	12.936	993.38	0.55	13.212	893.80	0.50	13.785	833.10	0.48
12.904	1038.07	0.57	13.362	995.42	0.55	13.606	897.17	0.51	14.139	837.31	0.48
13.327	1039.71	0.57	13.788	997.45	0.55	14.000	900.40	0.51	14.494	841.26	0.48
13.750	1041.31	0.57	14.214	999.50	0.55	14.394	903.44	0.51	14.849	844.88	0.48
14.173	1042.90	0.57	14.639	1001.46	0.55	14.788	906.45	0.51	15.203	849.44	0.48
14.596	1044.54	0.57	15.065	1003.43	0.55	15.182	909.27	0.51	15.558	853.17	0.49
15.019	1046.08	0.57	15.491	1005.37	0.56	15.576	912.32	0.51	15.913	856.71	0.49
15.442	1047.54	0.57	15.917	1007.25	0.56	15.970	915.21	0.51	16.267	860.21	0.49
15.865	1049.06	0.58	16.342	1009.13	0.56	16.364	917.94	0.52	16.622	863.48	0.49
16.288	1050.51	0.58	16.768	1010.91	0.56	16.758	920.64	0.52	16.977	866.80	0.49
16.711	1052.02	0.58	17.194	1012.70	0.56	17.152	923.23	0.52	17.348	870.10	0.49
17.135	1053.43	0.58	17.465	1013.86	0.56	17.546	925.79	0.52	17.703	873.19	0.50
17.558	1054.90	0.58	17.755	1015.03	0.56	17.940	928.37	0.52	18.075	876.31	0.50
17.981	1056.33	0.58	18.142	1016.64	0.56	18.334	930.88	0.52	18.446	879.36	0.50
18.404	1057.71	0.58	18.529	1018.20	0.56	18.728	933.38	0.52	18.801	882.26	0.50
18.827	1059.09	0.58	18.936	1019.78	0.56	19.015	935.11	0.52	19.156	884.97	0.50
19.250	1060.46	0.58	19.323	1021.27	0.56	19.373	937.24	0.52	19.426	887.01	0.50
19.673	1061.85	0.58	19.729	1022.82	0.56	19.731	939.35	0.52	19.747	889.44	0.50
20.000	1062.87	0.58	20.000	1023.79	0.56	20.000	940.84	0.53	20.000	891.26	0.50

FIGURES

(a)

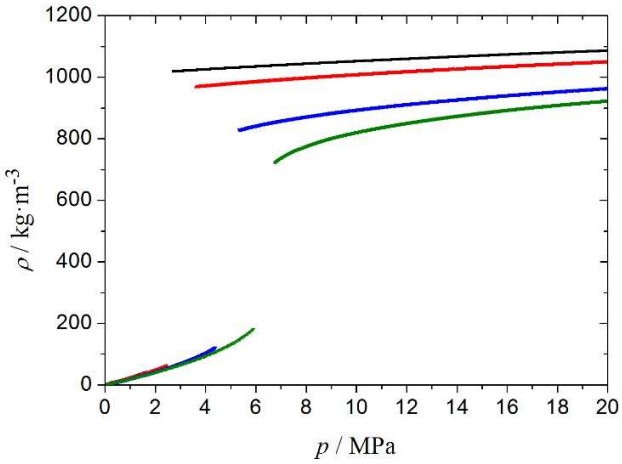

(b)

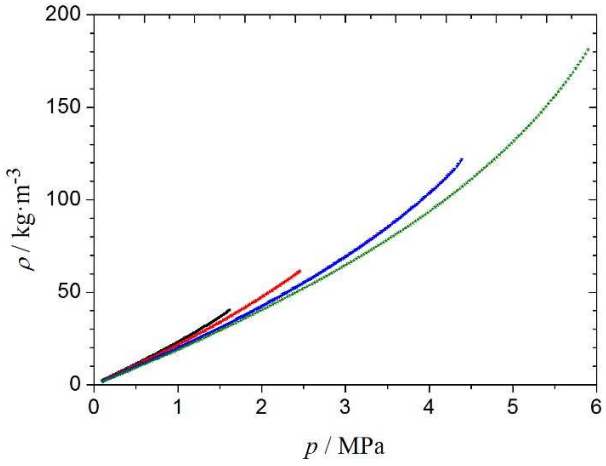

Figure 1. Experimental densities, ρ, of the CO_2+SO_2 mixture with $x_{CO_2} = 0.9532$ versus pressure, p, at several temperatures: (■), T = 263.15 K; (▲), T= 273.15 K; (▼), T = 293.15 K; and (★), T = 304.21 K. **(a)** Whole studied range of pressures. **(b)** Enlargement of the gas phase region.

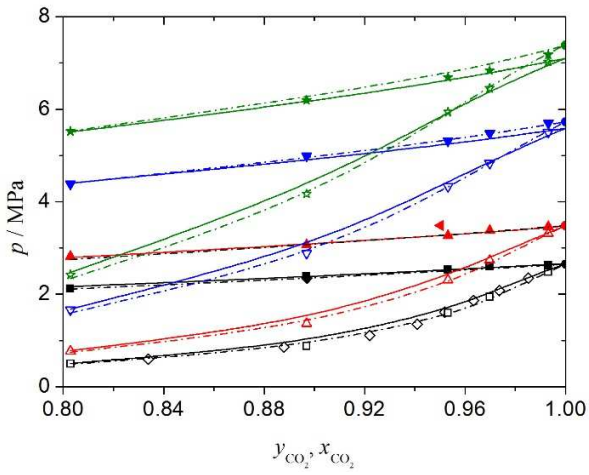

Figure 2. VLE for the CO_2+SO_2 system. Dew and bubble pressures versus composition of the vapor, y_{CO_2}, and liquid, x_{CO_2}, phases. Experimental data obtained in this work at several temperatures: (■), T = 263.15 K; (▲), T= 273.15 K; (▼), T = 293.15 K; and (★), T = 304.21 K. (◆), Experimental data at T = 263.15 K from Coquelet et al.[62] (◀), Experimental data at T = 273.56 K from Nazeri et al.[32] Empty symbols, dew points; full symbols, bubble points. Solid lines: PC-SAFT EoS using the coefficients from Table S8. Dashed-dotted lines: extended EOS-CG. Full circles: saturation pressures of pure CO_2 at 263.15 K (●), 273.15 (●), and 293.15 (●),[55] and critical pressure at 304.21 K (●).[56]

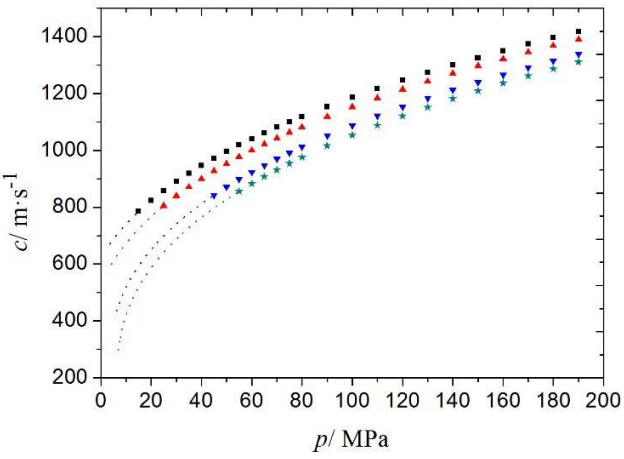

Figure 3. Experimental and extrapolated speed of sound, c, for the ternary CO_2+CH_3OH+SO_2 mixture with $x_{CO_2} = 0.9457$, $x_{CH_3OH} = 0.0075$ and $x_{SO_2} = 0.0468$ versus pressure, p, at several temperatures: (■), T = 263.15 K; (▲), T= 273.15 K; (▼), T = 293.15 K; and (★), T = 304.21 K. Symbols: experimental; dotted lines: extrapolated.

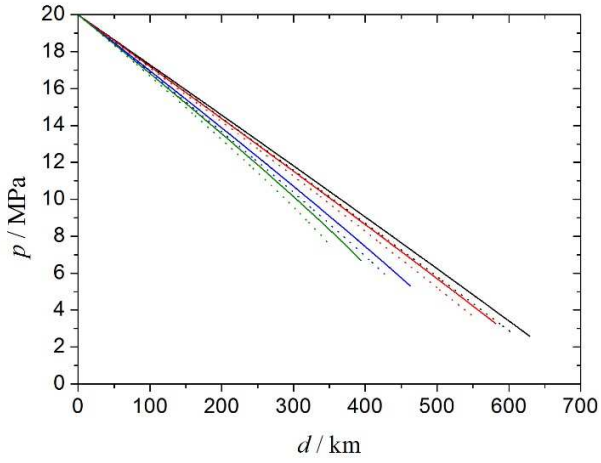

Figure 4. Comparison of pressure profiles along the pipeline for the CO_2+SO_2 mixture with $x_{CO_2} = 0.9532$ (solid lines) and pure CO_2 (dotted lines) at several transport temperatures: (—), T = 263.15 K; (—), T= 273.15 K; (—), T = 293.15 K; and (—), T = 304.21 K. Mass flow m =

317.1 kg/s, inner diameter of the pipeline D = 0.508 m, and roughness height e = 4.6×10^{-5} m were used along with a pipeline inlet pressure of 20.00 MPa.

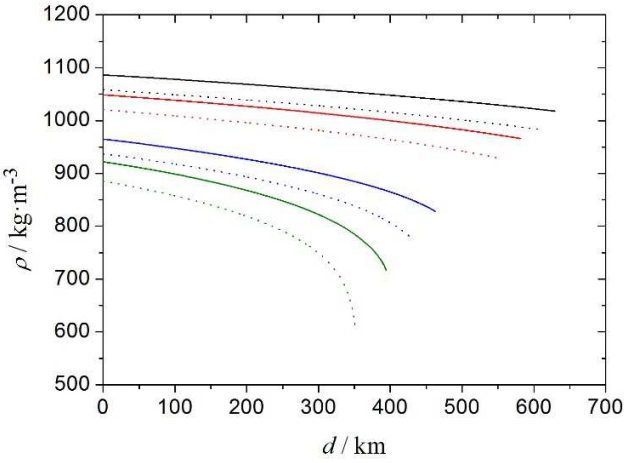

Figure 5. Comparison of density profiles along the pipeline for the CO_2+SO_2 mixture with x_{CO_2} = 0.9532 (solid lines) and pure CO_2 (dotted lines) at various transport temperatures: (—), T = 263.15 K; (—), T= 273.15 K; (—), T = 293.15 K; and (—), T = 304.21 K. Mass flow m = 317.1 kg/s, inner diameter of the pipeline D = 0.508 m, and roughness height e = 4.6×10^{-5} m were used along with a pipeline inlet pressure of 20.00 MPa.

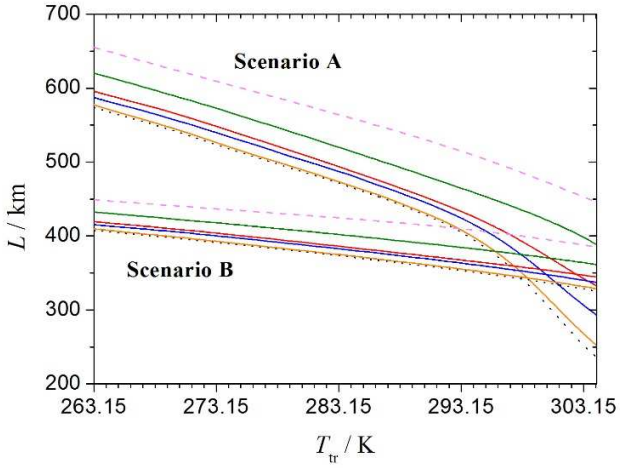

Figure 6. Maximum repressurization (pumping) distances, L, versus transport temperature, T_{tr}, for the CO_2+SO_2 studied mixtures and pure CO_2: (– – –), $x_{CO_2} = 0.8029$; (—), $x_{CO_2} = 0.8969$; (—), $x_{CO_2} = 0.9532$; (—), $x_{CO_2} = 0.9698$; (—), $x_{CO_2} = 0.9931$; (·····), pure CO_2. Scenario A: L required to maintain the pressure above p_{saf}. Scenario B: L required to maintain the pressure above 8.5 MPa. Mass flow was taken to be m = 317.1 kg/s, inner diameter of the pipeline D = 0.508 m, and roughness height $e = 4.6\times10^{-5}$ m. The pipeline inlet pressure was set at 20.00 MPa.

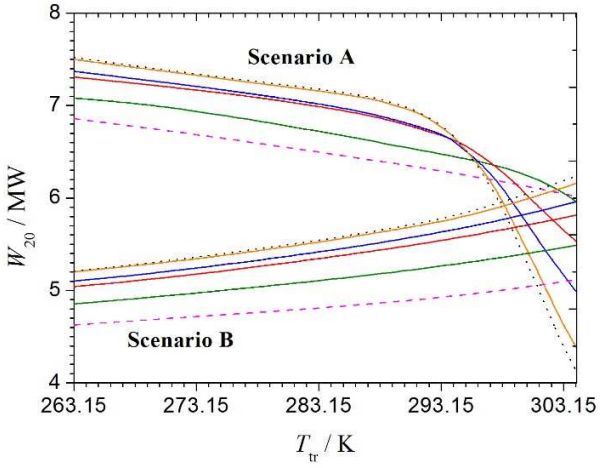

Figure 7. Booster station power, W_{20}, required to repressurize the fluid up to an outlet pressure and temperature of 20.00 MPa and 311 K versus the transport (= inlet) temperature, T_{tr}, for the CO_2+SO_2 studied mixtures and pure CO_2: (– – –), $x_{CO_2} = 0.8029$; (—), $x_{CO_2} = 0.8969$; (—), $x_{CO_2} = 0.9532$; (—), $x_{CO_2} = 0.9698$; (—), $x_{CO_2} = 0.9931$; (·····), pure CO_2. Scenario A: W_{20} necessary to repressurize from p_{saf} at T_{tr}. Scenario B: W_{20} necessary to repressurize from 8.5 MPa at T_{tr}. Mass flow was taken to be m = 317.1 kg/s, inner diameter of the pipeline D = 0.508 m, roughness height $e = 4.6\times10^{-5}$ m, and booster efficiency $y_{booster}$ = 0.75.

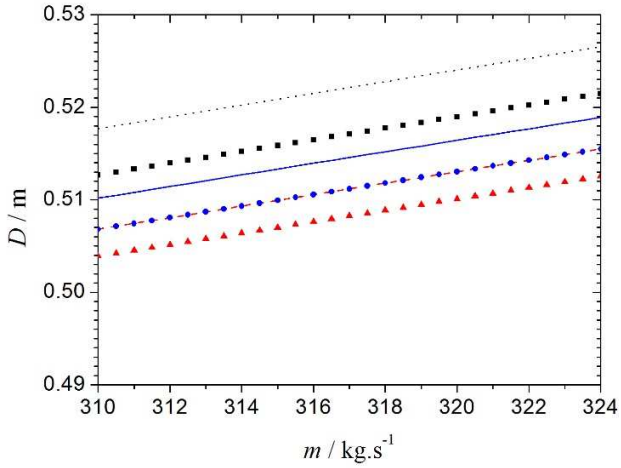

Figure 8. Pipeline inner diameter, *D*, versus mass flow (capacity), *m*, for the CO_2+SO_2 mixture with $x_{CO_2} = 0.9532$ and pure CO_2 at 293.15 K and the following pressures: (■, ····) 8.50 MPa; (●, −) 15.00 MPa, (▲, − · −) 20.00 MPa. Symbols, mixture; lines, pure CO_2. Roughness height was set at $e = 4.6\times10^{-5}$ m and an average value for pressure drop per meter of 30 $Pa\cdot m^{-1}$ was used.

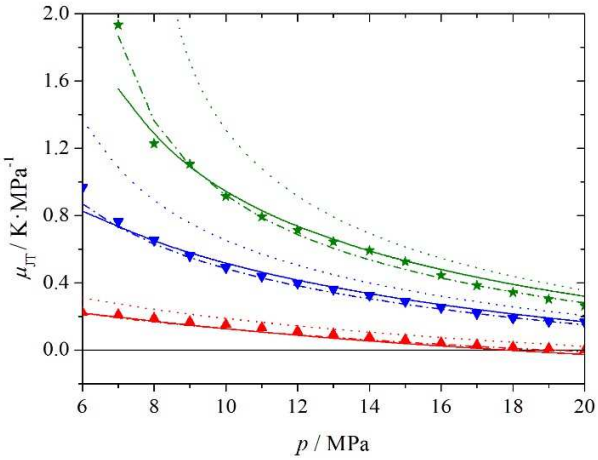

Figure 9. Calculated Joule-Thomson coefficient, μ_{JT}, at several pressures, p, and temperatures, T, for the CO_2+SO_2 mixture with x_{SO_2}= 0.0468, and for pure CO_2. Symbols, this work. Solid lines, PC-SAFT EoS using coefficients from Table S8. Dashed-dotted lines, extended EOS-CG. Dotted lines, pure CO_2.[55] (▲), T = 273.15 K; (▼), T = 293.15 K; and (★), T = 304.21 K.

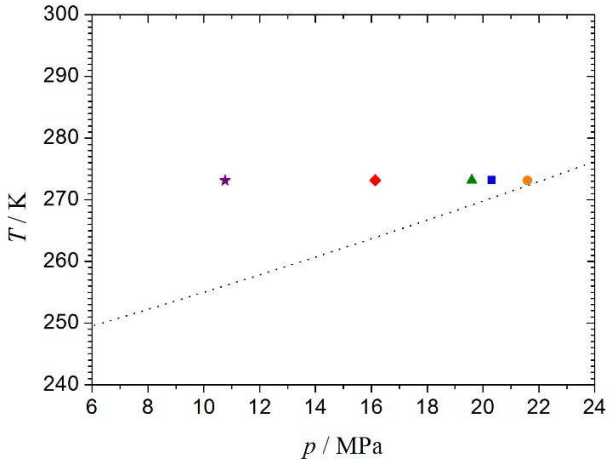

Figure 10. Joule-Thomson inversion pressures of the CO_2+SO_2 studied mixtures at 273.15 K and inversion line of pure CO_2.[55] Symbols, values calculated in this work for the mixtures: (●), $x_{SO_2} = 0.0069$; (■), $x_{SO_2} = 0.0302$; (▲), $x_{SO_2} = 0.0468$; (◆), $x_{SO_2} = 0.1031$; (★), $x_{CO_2} = 0.1917$.

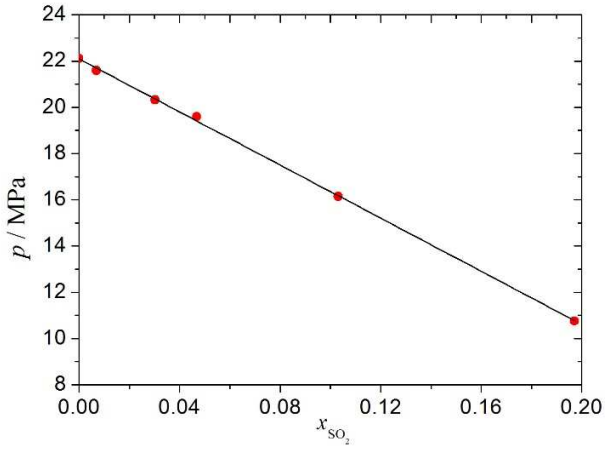

Figure 11. Correlation of the Joule-Thomson inversion pressures of the studied CO_2+SO_2 mixtures with the SO_2 mole fraction at 273.15 K. Data for pure CO_2 from Span and Wagner EoS[55] as implemented in REFPROP 9.1.[76]

ASSOCIATED CONTENT

Supporting Information.

The Supporting Information is available free of charge on the ACS Publications website at DOI:

Experimental and calculated data tables and additional figures as presented in the text (PDF).

AUTHOR INFORMATION

Corresponding Author

*Tel: +34 976761206. E-mail: javierf@unizar.es.

ORCID

Javier Fernández: 0000-0001-5256-6055

Beatriz Gimeno: 0000-0002-6992-5656

Manuela Artal: 0000-0003-1810-9488

Inmaculada Velasco: 0000-0001-6607-6858

Sofía T. Blanco: 0000-0003-2632-2916

Funding Sources

This work was supported by the Ministry of Economy and Competitiveness of Spain [ENE2013-44336-R], Government of Aragon [E32 23317/3], and University of Zaragoza [23321, 23326, 23327, 23328, and 23329].

Notes

The authors declare no competing financial interest.

ACKNOWLEDGMENTS

The authors acknowledge to their funding sources and thank Dr. Roland Span and Mr. Stefan Herrig for making the TREND 2.0.1 software available, and Dr. Luis Rández for computing assistance.

ABBREVIATIONS

CCS carbon capture and storage; VLE vapor-liquid equilibrium.

REFERENCES

(1) Dlugokencky, E.; Tans, P. NOAA/ESRL. Trends in atmospheric carbon dioxide. Web site. www.esrl.noaa.gov/gmd/ccgg/trends/ (accessed May 10, 2018).

(2) Hansen, J.; Sato, M.; Kharecha, P.; Beerling, D.; Berner, R.; Masson-Delmotte, V.; Pagani, M.; Raymo, M.; Royer, D. L.; Zachos, J. C. *et al*. Target atmospheric CO_2: Where should humanity aim? *Open Atmos. Sci. J.* **2008**, *2*, 217-231. http://dx.doi.org/10.2174/1874282300802010217.

(3) Allen, M. R.; Frame, D. J.; Huntingford, C.; Jones, C. D.; Lowe, J. A.; Meinshausen, M.; Meinshausen, N. Warming caused by cumulative carbon emissions towards the trillionth tonne. *Nature* **2009**, *458*, 1163-1166. http://dx.doi.org/10.1038/nature08019.

(4) *The Paris Agreement*; Framework Convention on Climate Change. United Nations. Web site. http://unfccc.int/paris_agreement/items/9485.php (accessed May 10, 2018)

(5) *The global Status of CCS: 2016*; Global CCS Institute; Melbourne, Australia. Web site. https://hub.globalccsinstitute.com/sites/default/files/publications/201158/global-status-ccs-2016-summary-report.pdf (accessed May 10, 2018).

(6) Figueroa, J. D.; Fout, T.; Plasynski, S.; McIlvried, H.; Srivastava, R. D. Advances in CO_2 capture technology - The US Department of Energy's Carbon Sequestration Program. *Int. J. Greenh. Gas Control* **2008**, *2* (1), 9-20. http://dx.doi.org/10.1016/S1750-5836(07)00094-1.

(7) MacDowell, N.; Florin, N.; Buchard, A.; Hallett, J.; Galindo, A.; Jackson, G.; Adjiman, C. S.; Williams, C. K.; Shahb, N.; Fennell, P. An overview of CO_2 capture technologies. *Energ. Environ. Sci.* **2010**, *3* (11), 1645-1669. http://dx.doi.org/10.1039/c004106h.

(8) Olajire, A. A. CO_2 capture and separation technologies for end-of-pipe applications - A review. 7th International Conference on Sustainable Energy Technologies. Liverpool, England, Feb 20-21, 2008.

(9) Bandyopadhyay, A.; Luo, G.; Fei, W. Preface. Special issue: CO_2 Capture and Storage. *Sep. Purif. Technol.* **2012**, *94*, 85-86. https://doi.org/10.1016/j.seppur.2012.02.012.

(10) Svenson, R.; Odenberger, M.; Johnsson, F.; Strömberg, L. Transportation infrastructure for CCS- Experiences and expected development. In *Greenhouse gas control technologies*; Wilson, M.; Morris, T.; Gale, J.; Thambimuthu, K., Eds.; Elsevier Ltd; 2005; Vol. II, pp 2531-2534.

(11) Doctor, R.; Palmer, A.; Coleman, D.; Davison, J.; Hendricks, C.; Kaarstad, O.; Ozaki, M.; Austell, M. Transport of CO_2. In *IPCC Special Report on Carbon Dioxide Capture and Storage*; Metz, B.; Davidson, O.; de Coninck, H.; Loos, M.; Meyer, L.; Eds.; Cambridge University Press, 2005; pp 179-193. Web site. https://www.ipcc.ch/report/srccs/ (accessed May 10, 2018)

(12) Zhang, Z. X.; Wang, G. X.; Massarotto, P.; Rudolph, V. Optimization of pipeline transport for CO_2 sequestration. *Energy Convers. Manag.* **2006**, *47*, 702-715. https://doi.org/10.1016/j.enconman.2005.06.001.

(13) McCoy, S. T.; Rubin, E. S. An engineering-economic model of pipeline transport of CO_2 with application to carbon capture and storage. *Int. J. Greenh. Gas Control* **2008**, *2*, 219-229. https://doi.org/10.1016/S1750-5836(07)00119-3.

(14) Knoope, M. M. J.; Ramírez, A.; Faaij, A. P. C. A state-of-the-art review of techno-economic models predicting the costs of CO_2 pipeline transport. *Int. J. Greenh. Gas Control* **2013**, *16* (1), 241-270. https://doi.org/10.1016/j.ijggc.2013.01.005.

(15) Knoope, M. M. J.; Guijt, W.; Ramírez, A.; Faaij, A. P. C. Improved cost models for optimizing CO2 pipeline configuration for point-to-point pipelines and simple networks. *Int. J. Greenh. Gas Control* **2014**, *22* (1), 25-46. http://dx.doi.org/10.1016/j.ijggc.2013.12.016.

(16) *Geologic Storage of Carbon Dioxide*; International Energy Agency; Greenhouse Gas R&D Programme, January 2008. Web site.

http://www.ccsassociation.org/docs/2008/IEA%20GHG%20geological%20storage%20of%20CO2%20February%2008.pdf (accessed May 10, 2018).

(17) *Energy Technology Perspectives 2017: Catalysing Energy Technology Transformations*; International Energy Agency, 2017. Web site. https://www.iea.org/publications/freepublications/publication/EnergyTechnologyPerspectives2017ExecutiveSummaryEnglishversion.pdf (accessed May 10, 2018).

(18) *The global Status of CCS: 2017*; Global CCS Institute, 2017. Web site. http://www.globalccsinstitute.com/sites/www.globalccsinstitute.com/files/uploads/global-status/1-0_4529_CCS_Global_Status_Book_layout-WAW_spreads.pdf (accessed May 10, 2018).

(19) *World Energy Outlook 2009*; International Energy Agency, 2009. Web site. http://www.worldenergyoutlook.org/media/weowebsite/2009/WEO2009.pdf (accessed May 10, 2018)

(20) CO_2 Pipeline Infrastructure. International Energy Agency 2014. IEAGHG Report 2013/18, January 2014. Web site. http://ieaghg.org/docs/General_Docs/Reports/2013-18.pdf (accessed May 10, 2018).

(21) Løvseth, S.; Skaugen, G.; Stang, H. G. J.; Jakobsen, J. P.; Wilhelmsen, Ø.; Span, R.; Wegge, R. CO_2 Mix Project: Experimental determination of thermophysical properties of CO_2-rich mixtures. *Energy Procedia* **2013**, *37*, 2889-2896. http://dx.doi.org/10.1016/j.egypro.2014.09.002.

(22) Porter, R. T. J.; Fairweather, M.; Pourkashanian, M.; Woolley, R. M. The range and level of impurities in CO_2 streams from different carbon capture sources. *Int. J. Greenh. Gas Control* **2015**, *36*, 161-174. http://dx.doi.org/10.1016/j.ijggc.2015.02.016.

(23) Wang, J.; Ryan, D.; Anthony, E. J.; Wildgust, N.; Aiken, T. Effects of Impurities on CO_2 Transport, Injection and Storage. *Energy Procedia* **2011**, *4*, 3071-3078. http://dx.doi.org/10.1016/j.egypro.2011.02.219.

(24) Ziabakhsh-Ganji, Z.; Kooi, H. Sensitivity of the CO_2 storage capacity of underground geological structures to the presence of SO_2 and other impurities. *Appl. Energy* **2014,** *135*, 43-52. http://dx.doi.org/10.1016/j.apenergy.2014.08.073.

(25) Koenen, M.; Waldmann, S.; Hofstee, C.; Neele, F. Effect of SO_2 co-injection on CO_2 storage. Presented at 2nd International Forum on Recent Developments of CCS Implementations, Athens, 16th-17th December, 2015.

(26) Wang, J.; Wang, Z. Y.; Ryan, D.; Lan, C. A study of the effect of impurities on CO_2 storage capacity in geological formations. *Int. J. Greenh. Gas Control* **2015**, *42*, 132-137. http://dx.doi.org/10.1016/j.ijggc.2015.08.002.

(27) Ziabakhsh-Ganji, Z. Physical and geochemical impacts of impure CO_2 on storage in depleted hydrocarbon reservoirs and saline aquifers. Ph.D. Thesis, University of Amsterdam, the Netherlands, 2015.

(28) Crandell, L. E.; Ellis, B. R.; Peters, C. A. Dissolution Potential of SO_2 Co-Injected with CO_2 in Geologic Sequestration. *Environ. Sci. Technol.* **2010**, *44*, 349-355. http://dx.doi.org/10.1021/es902612m.

(29) Xiang, Y.; Wang, Z.; Yang, X.; Li, Z.; Ni, W. The upper limit of moisture content for supercritical CO2 pipeline transport. *J. Supercrit. Fluids* **2012**, *67*, 14-21. https://doi.org/10.1016/j.supflu.2012.03.006.

(30) Miri, R.; Aagaard, P.; Hellevang, H. Examination of CO_2-SO_2 Solubility in Water by SAFT1. Implications for CO_2 Transport and Storage. *J. Phys. Chem. B* **2014**, *118* (34), 10214-10223. http://dx.doi.org/10.1021/jp505562j.

(31) Kim, M. C.; Song, K. H. Effect of impurities on the onset and growth of gravitational instabilities in a geological CO_2 storage process: Linear and nonlinear analyses. *Chem. Eng. Sci.* **2017**, *174*, 426-444. https://doi.org/10.1016/j.ces.2017.09.038.

(32) Nazeri, M.; Chapoy, A.; Valtz, A.: Coquelet, C.; Tohidi, B. New experimental density data and derived thermophysical properties of carbon dioxide - Sulphur dioxide binary mixture (CO_2 - SO_2) in gas, liquid and supercritical phases from 273 K to 353 K and at pressures up to 42 MPa. *Fluid Phase Equilibr.* **2017**, *454*, 64-77. https://doi.org/10.1016/j.fluid.2017.09.014.

(33) Rivas, C.; Gimeno, B.; Artal, M.; Blanco, S. T.; Fernández, J.; Velasco, I. High-pressure speed of sound in pure CO_2 and in CO_2 with SO_2 as an impurity using methanol as a doping agent. *Int. J. Greenh. Gas Control* **2016**, *54*, 737-751. http://dx.doi.org/10.1016/j.ijggc.2016.09.014.

(34) Gimeno, B.; Artal, M.; Velasco, I.; Blanco, S. T.; Fernández J. Influence of SO_2 on CO_2 storage for CCS technology: Evaluation of CO_2/SO_2 co-capture. *Appl. Energy* **2017**, *206*, 172-180. https://doi.org/10.1016/j.apenergy.2017.08.048.

(35) Gross, J.; Sadowski, G. Perturbed-Chain SAFT: An Equation of State based on a perturbation theory for chain molecules. *Ind. Eng. Chem. Res.* **2001**, *40* (4), 1244-1260. http://dx.doi.org/10.1021/ie0003887 .

(36) Gernert, J; Span, R. EOS-CG: A Helmholtz energy mixture model for humid gases and CCS mixtures. *J. Chem. Thermodyn.* **2016**, *93*, 274-293. http://dx.doi.org/10.1016/j.jct.2015.05.015.

(37) Span, R.; Eckermann, T.; Herrig, S.; Hielscher, S.; Jäger, A.; Thol, M. TREND. Thermodynamic Reference and Engineering Data 2.0.1. Lehrstuhl fuer Thermodynamik, Ruhr-Universitaet Bochum, 2015.

(38) Cole, I. S.; Corrigan, P.; Sim, S.; Birbilis, N. Corrosion of pipelines used for CO_2 transport in CCS: Is it a real problem? *Int. J. Greenh. Gas Control* **2011**, *5*, 749-756. http://dx.doi.org/10.1016/j.ijggc.2011.05.010.

(39) Dugstad, A.; Morland, B.; Clausen, S. Corrosion of transport pipelines for CO_2 – effect of water ingress. *Energy Procedia* **2011**, *4*, 3063-3070. http://dx.doi.org/10.1016/j.egypro.2011.02.218.

(40) Xiang, Y.; Wang, Z.; Xu, C.; Zhou, C.; Li, Z.; Ni, W. Impact of SO_2 concentration on the corrosion rate of X70 steel and iron in water-saturated supercritical CO_2 mixed with SO_2. *J. Supercrit. Fluids* **2011**, *58*, 286-294. https://doi.org/10.1016/j.supflu.2011.06.007.

(41) Paschke, B.; Kather, A. Corrosion of Pipeline and Compressor Materials due to Impurities in separated CO_2 from fossil-fuelled Power Plants. *Energy Procedia* **2012**, *23*, 207-215. http://dx.doi.org/10.1016/j.egypro.2012.06.030.

(42) Rhul, A. S.; Kranzmann, A. Corrosion in supercritical CO_2 by diffusion of flue gas acids and water. *J. Supercrit. Fluids* **2012**, *68*, 81-86. https://doi.org/10.1016/j.supflu.2012.04.015.

(43) Dugstad, A.; Halseid, M.; Morland, B. Effect of SO_2 and NO_2 on corrosion and solid formation in dense phase CO_2 pipelines. *Energy Procedia* **2013**, *37*, 2877-2887. http://dx.doi.org/10.1016/j.egypro.2013.06.173.

(44) Farelas, F.; Choi, Y. S.; Nešić, S. Corrosion Behavior of API 5L X65 Carbon Steel Under Supercritical and Liquid Carbon Dioxide Phases in the Presence of Water an Sulfur Dioxide. *Corrosion* **2013**, *69* (3), 243-250. http://dx.doi.org/10.5006/0739.

(45) Brown, J.; Graver, B.; Gulbrandsen, E.; Dugstad, A.; Morland, B. Update of DNV recommended practice RP-J202 with focus on CO_2 Corrosion with Impurities. *Energy Procedia* **2014**, *6*, 2432-2441. http://dx.doi.org/10.1016/j.egypro.2014.11.265.

(46) Hua, Y.; Barker, R.; Neville, A. The influence of SO_2 on the tolerable water content to avoid pipeline corrosion during the transportation of supercritical CO_2. *Int. J. Greenh. Gas Control* **2015**, *37*, 412-423. https://doi.org/10.1016/j.ijggc.2015.03.031.

(47) Velasco, I.; Rivas, C.; Martínez-López, J. F.; Blanco, S. T.; Otín, S.; Artal, M. Accurate values of some thermodynamic properties for carbon dioxide, ethane, propane, and some binary mixtures. *J. Phys. Chem. B* **2011**, *115* (25), 8216-8230. http://dx.doi.org/10.1021/jp202317n.

(48) Blanco, S. T.; Rivas, C.; Bravo, R.; Fernández, J.; Artal, M.; Velasco, I. Discussion on the influence of CO and CH_4 in CO_2 transport, injection, and storage for CCS technology. *Environ. Sci. Technol.* **2014**, *48* (18), 10984–10992. http://dx.doi.org/10.1021/es502306k.

(49) Procedimiento TH-006 para la calibración de termómetros de resistencia de platino. Área de Temperatura. Centro Español de Metrología. Ministerio de Industria, Turismo y Comercio. Editorial/NIPOP/ISBN: 165-00-006-1; 2000.

(50) Bouchot, C.; Richon, D. Direct pressure-volume-temperature and vapor-liquid equilibrium measurements with a single equipment using a vibrating tube densimeter up to 393 K and 40 MPa: Description of the original apparatus and new data. *Ind. Eng. Chem. Res.* **1998**, *37* (8), 3295-3304. http://dx.doi.org/10.1021/ie970804w.

(51) Li, H.; Jakobsen, J. P.; Wilhelmsen, Ø.; Yan, J. PVTxy properties of CO_2 mixtures relevant for CO_2 capture, transport and storage: Review of available experimental data and theoretical models. *Appl. Energy* **2011**, *88* (11), 3567-3579. http://dx.doi.org/10.1016/j.apenergy.2011.03.052.

(52) Serpa, J.; Morbee, J.; Tzimas, E. *Technical and Economic Characteristics of a CO_2 Transmission Pipeline Infrastructure;* European Commission; Joint Research Centre; Institute of Energy, 2011. JRC62502. Web site. http://publications.jrc.ec.europa.eu/repository/bitstream/111111111/16038/1/reqno_jrc62502_aspublished.pdf (accessed May 10, 2018).

(53) *Annual European Union greenhouse gas inventory 1990–2015 and inventory report 2017*; EEA Report No 6/2017; European Environment Agency, 2017. Web site. https://www.eea.europa.eu/publications/european-union-greenhouse-gas-inventory-2017 (accessed May 10, 2018).

(54) *Inventory of U.S. greenhouse gas emissions and sinks: 1990 – 2015*; EPA 430-P-17-001; U.S. Environmental Protection Agency, 2017. Web site. https://www.epa.gov/ghgemissions/inventory-us-greenhouse-gas-emissions-and-sinks-1990-2015 (accessed May 10, 2018).

(55) Span, R.; Wagner, W. A new equation of state for carbon dioxide covering the fluid region from the triple-point temperature to 1100 K at pressures up to 800 MPa. *J. Phys. Chem. Ref. Data* **1996**, *25* (6), 1509-1596. https://doi.org/10.1063/1.555991.

(56) Gil, L.; Otin, S. F.; Muñoz Embid, J.; Gallardo, A.; Blanco, S. T.; Artal, M.; Velasco, I. Experimental setup to measure critical properties of pure and binary mixtures and their densities at different pressures and temperatures. Determination of the precision and uncertainty in the results. *J. Supercrit. Fluids* **2008**, *44*, 123-138. http://dx.doi.org/10.1016/j.supflu.2007.11.003.

(57) Blümcke, A. Ueber die Bestimmung der specifischen Gewichte und Dampfspannungen einiger Gemische von schwefliger Säure und Kohlensäure. *Ann. Phys-Leipzig.* **1888**, *270* (5), 10-21. http://dx.doi.org/10.1002/andp.18882700503.

(58) Caubet, F. Liquéfaction des mélanges gazeux. Ph.D. Thesis, Université de Bordeaux, France, 1901.

(59) Thiel, A.; Schulte, E. Über binäre Gleichgewichtssysteme mit festem Kohlendioxyd. *Z. Phys. Chem-Stoch Ve.* **1920**, *96* (3/4), 312-342. https://doi.org/10.1515/zpch-1920-9611.

(60) Cummings, L. W. T. High-pressure rectification I - Vapor-liquid equilibrium relations at high pressures. *Ind. Eng. Chem.* **1931**, *23*, 900-902. https://doi.org/10.1021/ie50260a010.

(61) Lachet, V.; de Bruin, T.; Ungerer, P.; Coquelet, C.; Valtz, A.; Hasanov, V.; Lockwood, F.; Richon, D. Thermodynamic behavior of the CO_2 + SO_2 mixture: experimental and Monte Carlo simulation studies. *Energy Procedia* **2009**, *1* (1), 1641-1647. http://dx.doi.org/10.1016/j.egypro.2009.01.215.

(62) Coquelet, C.; Valtz, A.; Arpentinier, P. Thermodynamic study of binary and ternary systems containing CO_2 + impurities in the context of CO_2 transportation. *Fluid Phase Equilibr.* **2014**, *382*, 205-211. http://dx.doi.org/10.1016/j.fluid.2014.08.031.

(63) ThermoLit. NIST Literature Report Builder for Thermophysical and Thermochemical Property Measurements. NIST Standard Reference Database #171. Web site. http://trc.nist.gov/thermolit/main/home.html#home (accessed May 10, 2018).

(64) Wilhelmsen, Ø.; Skaugen, G.; Jørstad, O.; Li, H. Evaluation of SPUNG and other Equations of State for use in Carbon Capture and Storage modelling. *Energy Procedia* **2012**, *23*, 236-245. http://dx.doi.org/10.1016/j.egypro.2012.06.024.

(65) Diamantonis, N. I.; Boulougouris., G. C.; Tsangaris, D. M.; El Kadi, M.; Saadawi, H.; Economou, I. G. Thermodynamic and transport property models for carbon capture and sequestration (CCS) processes with emphasis on CO_2 transport. *Chem. Eng. Res. Des.* **2013**, *91* (10), 1793-1806. http://dx.doi.org/10.1016/j.cherd.2013.06.017.

(66) Seevam, P. N.; Race, J. M.; Downie, J. M.; Hopkins P. Transporting the next generation of CO_2 for carbon, capture and storage: the impact of impurities on supercritical CO_2 pipelines. Proceedings of IPC2008, 7th International Pipeline Conference, Calgary, Alberta, Canada, September 29-October 3, 2008; IPC2008-64063.

(67) Kunz, O.; Klimeck, R.; Wagner, W.; Jaeschke, M. *The GERG 2004 Wide range equation of state for natural gases and other mixtures*; Technical Monograph GERG TM15 2007. VDI-Verlag GmbH; Dusseldorf, Germany, 2007.

(68) Gao, K.; Wu, J.; Zhang, P.; Lemmon, E. W. A Helmholtz Energy Equation of State for Sulfur Dioxide. J. Chem. Eng. Data **2016**, *61* (8), 2859-2872. http://dx.doi.org/10.1021/acs.jced.6b00195.

(69) Laursen, T. VLXE ApS. Scion-DTU, Diplomvej, Denmark, 2012.

(70) Rivas, C.; Blanco, S. T.; Fernández, J.; Artal, M.; Velasco, I. Influence of methane and carbon monoxide in the volumetric behaviour of the anthropogenic CO_2: Experimental data and modelling in the critical region. *Int. J. Greenh. Gas Control* **2013**, *18*, 264-276. http://dx.doi.org/10.1016/j.ijggc.2013.07.019.

(71) Diamantonis, N. I.; Boulougouris, G. C.; Mansoor, E.; Tsangaris, D. M.; Economou, I. G. Evaluation of cubic, SAFT, and PC-SAFT equations of state for the vapor-liquid equilibrium modeling of CO_2 mixtures with other gases. *Ind. Eng. Chem. Res.* **2013**, *52* (10), 3933-3942. http://dx.doi.org/10.1021/ie303248q.

(72) Xu, X.; Privat, R.; Jaubert, J. N.; Lachet, V.; Creton, B. Phase equilibrium of CCS mixtures: Equation of state modeling and Monte Carlo simulation. *J. Supercrit. Fluid* **2017**, *119*, 169-202. http://dx.doi.org/10.1016/j.supflu.2016.09.013.

(73) Vandeginste, V.; Piessens, K. Pipeline design for a least - cost router application for CO_2 transport in the CO_2 sequestration cycle. *Int. J. Greenh. Gas Control* **2008**, *2* (4), 571-581. http://dx.doi.org/10.1016/j.ijggc.2008.02.001.

(74) *ElementEnergy, 2010. CO_2 pipeline infrastructure*; *An analysis of global challenges and opportunities*; Final report for IEA Greenhouse Gas Programme, 27/04/2010. Web site. http://www.ccsassociation.org/docs/2010/IEA%20Pipeline%20final%20report%20270410.pdf (accessed May 10, 2018).

(75) Klein, S. A.; McLinden, M. O.; Laesecke, A. An improved extended corresponding states method for estimation of viscosity of pure refrigerants and mixtures. *Int. J. Refrig.* **1997**, *20*, 208-217. http://dx.doi.org/10.1016/S0140-7007(96)00073-4.

(76) Lemmon, E. W.; Huber, M. L.; McLinden, M. O. Reference Fluid Thermodynamic and Transport Properties-REFPROP. NIST Standard Reference Database 23, Version 9.1, DLL version number 9.1. U.S. Secretary of Commerce on behalf of the United States of America; 2013.

(77) Farris, C. B. Unusual Design Factors for Supercritical CO_2 Pipelines. *Energy Prog.* **1983**, *3* (3), 150-158.

(78) Mohitpour, M.; Jenkins, A.; Nahas, G. A generalized overview of requirements for the design, construction, and operation of new pipelines for CO_2 sequestration. *J. Pipeline Eng.* **2008**, *7* (4), 237-251. Web site. http://www.j-pipe-eng.com/Abstract.cfm?cat_no=2148s (accessed May 10, 2018).

(79) Witkowski, A.; Rusin, A.; Majkut, M.; Rulic, S.; Stolecka, K. Comprehensive analysis of pipeline transportation systems for CO_2 sequestration. Thermodynamics and safety problems. *Energy Convers. Manag.* **2013**, *76*, 665-673. https://doi.org/10.1016/j.enconman.2013.07.087